DENSITY FUNCTIONAL THEORY (DFT) STUDY OF HYDROGEN STORAGE

IN POROUS SILICON

A Thesis

Submitted to the Faculty

of

Purdue University

by

Mawla Boaks

In Partial Fulfillment of the

Requirements for the Degree

of

Master of Science in Electrical and Computer Engineering

May 2018

Purdue University

Indianapolis, Indiana

THE PURDUE UNIVERSITY GRADUATE SCHOOL
STATEMENT OF COMMITTEE APPROVAL

Dr. Peter J. Schubert, Chair

    Department of Electrical and Computer Engineering

Dr. Maher E. Rizkalla

    Department of Electrical and Computer Engineering

Dr. Mangilal Agarwal

    Department of Mechanical and Energy Engineering

Approved by:

    Dr. Brian King

        Head of the Graduate Program

I dedicate my master's thesis to my lovely wife Sahlil Ahmed, who spent sleepless nights back home taking care of our only child while I was 8000 miles away.

ACKNOWLEDGMENTS

TABLE OF CONTENTS

LIST OF TABLES

LIST OF FIGURES

SYMBOLS

m	mass
v	velocity
ψ	wave function
q	charge
E	energy
$\hat{H}$	hamiltonian
U	potential
V	potential
$n(r)$	electron density
H	hessian matrix
λ	eigen value
e	eigen vector
h	plank's constant
ν	vibrational frequency
$\mathbf{A}$	mass weighted hessian matrix
$\dagger$	transition state
T	temperature

ABBREVIATIONS

DFT   Density Functional Theory

npSi   Nanoporous Silicon

Pd   Palladium

Si   Silicon

BZ   Brillouin Zone

LDA   Local Density Approximation

GGA   Generalized Gradient Approximation

Ha   Hartree

SCF   Self Consistent Field

NEB   Nudged Elastic Band

CI-NEB Climbing-Image Nudged Elastic Band

GS   Ground State

MEP   Minimum Energy Path

ABSTRACT

Boaks, Mawla. M.S.E.C.E., Purdue University, May 2018. Density Functional Theory (DFT) Study of Hydrogen Storage in Porous Silicon. Major Professor: Peter J. Schubert.

Based on plane wave DFT calculation, we carried out micro level investigation of hydrogen storage in nanoporous silicon (npSi). One quarter of a hexagonal pore with Palladium catalyst placed at the surface has been studied for hydrogen dissociation, spillover, bond hopping, and diffusion for both single catalyst atom and small catalyst cluster consisting of multiple catalyst atoms. All the DFT computations were done in one of the biggest research supercomputer facilities of the world, Big Red II. We opted ABINIT, an open source DFT tool for our computations. Our calculation revealed low dissociation, spillover, and bond hoping energy barrier. The energy required to be provided from external sources to fully recharge the storage medium from a gaseous source at a completely empty state has also been evaluated. Hydrogen diffusion along the inner surface of the pore as a means of bond hopping and the possibility of quantum tunneling, a low temperature phenomena used to spontaneously go over an otherwise less likely high energy barrier have been studied as well. Using these micro level parameter values evaluated from the DFT study, the performance of any potential hydrogen storage material can be compared to a set of characteristics sought in an efficient storage media. Thus, the micro scale feasibility of this novel npSi material based hydrogen storage technology was studied as a part of a STTR Phase I project.

1. INTRODUCTION

1.1 Hydrogen Storage in Porous Silicon

Hydrogen is a clean and renewable source of energy [1] [2]. Hydrogen has potential to be used as an alternative to traditional energy sources in near future. But it will require a safe, cheap, and effective storage media to boost hydrogen as an energy carrier. The first sought characteristics in a hydrogen storage media is its high storage capability with H_2 weight >6.0 wt.%. Nanoporous silicon synthesized in electrochemical etching procedure from bulk silicon has shown theoretical hydrogen storage capacity up to 6.6 wt.% [3]. Silicon is abundant and benign in nature. The second required criteria in a storage media is hydrogen adsorption and desorption in ambient or near ambient conditions [4]. Thirdly, reversible hydrogen releasing is expected of a hydrogen storage medium. A NSF grant (grant number: 1648748) was awarded to Green Fortress Engineering, Inc. to study if porous silicon based hydrogen storage media has these mentioned characteristics [5]. This thesis work was pursued to do micro scale study as a part of this NSF project. A relevant but out of the scope of this thesis mass transport model was developed to compare the performance of this nanoporous silicon based hydrogen storage medium against those requirements. For this macroscopic mass transport model, we have evaluated some of the micro level parameters using density functional theory (DFT) that approximates the solution of the many body Schrödinger equation. The mass transport model calculates the hydrogen concentration and recharge time depending on pressure and temperature. Thus, the model should be able to assess nanoporous silicon as a potential hydrogen storage media.

In this system, hydrogen goes through a series of equilibrium reactions that form different types of compounds that bond silicon and hydrogen. At the beginning, molecular hydrogen is split into atomic hydrogen ions by the palladium catalyst, which the ions then dissociate onto.

$$H_2 \leftrightarrow 2H_{Pd}^+$$
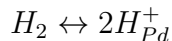
These hydrogen ions then bond onto dangling bonds on the silicon, creating the Si-H bonds that form the backbone of the porous silicon storage medium.

$$H_{Pd}^+ + Si^* \rightarrow SiH$$
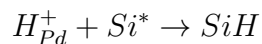
The net chemical reaction is as follows:

$$H_2 + 2Si^* \leftrightarrow 2SiH$$
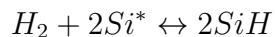
The hydrogen atoms hop from one silicon dangling bond to the other and thus diffusion takes place along the inner silicon surface of the pore. In this micro level study, we have thereby investigated hydrogen dissociation, spillover, bond hopping, and diffusion within the computational framework of DFT.

1.2   Density Functional Theory

In order to describe the properties of a collection of atoms we are mainly after the ground state energy for the well-defined collection of atoms. We can find the ground state by solving many body Schrödinger equation for that collection of atoms:

$$\hat{H}\psi(\{r_i\}, \{R_I\}) = E\psi(\{r_i\}, \{R_I\}) \tag{1.1}$$

ψ is the wave function here which describes our system of atoms consisting of nucleus and electrons. r_i and R_I represent the positions of electrons and nuclei respectively. Hamiltonian, $\hat{H}$ is an energy operator operating on our wave function. The energy operator can be broken into two parts:

$$\hat{H} = \hat{T} + \hat{V}_{coulomb} \tag{1.2}$$

$\hat{T}$ and $\hat{V}_{coulomb}$ are the kinetic energy operator and coulomb potential operator respectively. The coulomb potential operator includes all the coulomb interactions between charges (ie: Nuclei-Nuclei, electron-Nuclei, electron-electron). Therefore,

$$\hat{V}_{coulomb} = \frac{q_i q_j}{|r_i - r_j|} \tag{1.3}$$

Here, there are bunches of electrons and nucleus which interact with one another. This makes the Schrödinger equation difficult to solve. To make this equation a little bit simpler to solve, we apply the Born-Oppenheimer approximation. The nuclei are substantially heavier and slower compared to the electrons. Electrons are relatively faster than nuclei and they take considerably lesser time to go to the lowest energy state or ground state of electrons for fixed position of nuclei. As a result, the electrons see the nuclei as external potential of fixed nuclei.

$$m_{nuclei} >> m_e \tag{1.4}$$

According to the Born-Oppenheimer approximation, the dynamics of atomic nuclei and electrons can be separated as follows:

$$\psi(\{r_i\}, \{R_I\}) = \psi_N(\{R_I\}) * \psi_e(\{r_i\}) \tag{1.5}$$

So, we will be concentrating on first solving only the ground state of electrons for fixed set of nuculei. Thus, we have reduced the number of variables in the Schrödinger equation and it looks file follows:

$$\hat{H}\psi(r_1, r_2, r_3, ..., r_N) = E\psi(r_1, r_2, r_3, ..., r_N) \tag{1.6}$$

Hamiltonian, $\hat{H}$ only consists of three terms accordingly:

$$\hat{H} = \left[-\frac{\hbar^2}{2m_e} \sum_{i=1}^{N_e} \nabla_i^2 + \sum_{i=1}^{N_e} V_{ext}(r_i) + \sum_{i=1}^{N_e} \sum_{j>1} U(r_i, r_j) \right] \tag{1.7}$$

The first term in the right hand side denotes the kinetic energy of the electrons, second term denotes the potential due to interaction between the electrons and external nuclei and finally the third term denotes electron-electron repulsion.

Even after Born-Oppenheimer approximation, this is still a high dimensional problem to be solved. Here, the electron wave function, ψ is still a function of all three spatial coordinates of each of the electrons. In our porous silicon matrix that comprises only quarter of a pore, there are 340 silicon atoms. Each silicon atom has 14 electrons. Therefore, Schrödinger equation of our quarter pore silicon matrix alone is 14280 ($340 \times 14 \times 3$) dimensional problem. In order to reduce the complexity of this problem, we switch to electron density from electron wave function. The electron density is a true observable unlike the electron wave function. The electron density, n(r) is a function of only 3 dimension unlike the electron wave function ψ which is the function of all three spatial coordinates of each of the electrons. Therefore, the dimension of the problem reduces to 3 from 3N. The electron density is defined as the probability that the N electrons are at particular set of coordinates, r_1, ..., r_N. Hence,

$$n(r) = \psi^*(r_1, r_2, ..., r_N)\psi(r_1, r_2, ..., r_N) \tag{1.8}$$

If we consider any electron as a point charge located in the field of all other electrons, we will be able to simplify the many electron problem into many one electron problems. So, we consider single electron wave functions:

$$\psi(r_1, r_2, ..., r_N) = \psi_1(r_1) * \psi_2(r_2) * \psi_3(r_3) * .... * \psi_N(r_N) \tag{1.9}$$

We can re-define our electron density in terms of single electron wave functions:

$$n(r) = 2 \sum_i \psi_i^*(r)\psi_i(r) \tag{1.10}$$

Hohenberg and Kohn provided two theorems that is at the center of DFT. Theorem 1 states that the ground state energy is an unique functional of electron density.

$$E = E[n(r)] \tag{1.11}$$

In general words, if we find the electron density that will lead to total ground state energy. Theorem 2 states that the electron density that minimizes the energy of the overall functional is the true electron density corresponding to the full solution of Schrödinger equation.

$$E[n(r)] > E_0[n_0(r)] \tag{1.12}$$

Here, E_o and $n_0(r)$ are minimum of the energy functional and ground state electron density respectively. The energy functional can be broken into two parts: known and unknown.

$$E\left[\{\psi_i\}\right] = E_{known}\left[\{\psi_i\}\right] + E_{XC}\left[\{\psi_i\}\right] \tag{1.13}$$

The known parts consists of the kinetic energy and the potential energy terms arising due to coulomb interactions.

$$E_{known}\left[\{\psi_i\}\right] = -\frac{\hbar^2}{m_e}\sum_i \int \psi_i^* \nabla^2 \psi_i d^3r + \int V(r)n(r)d^3r + \frac{e^2}{2} \int \int \frac{n(r)n(r')}{|r-r'|}d^3rd^3r'$$
$$+ E_{ion} \quad (1.14)$$

The unknown part consists of the exchange correlation functional including all the quantum mechanical interaction between electrons. The exchange correlation functional is not known and they are approximated. There are two types of exchange correlation functional commercial DFT packages utilize. One is the LDA or local density approximation based on local electron density, the second one is GGA or generalized gradient approximation based on gradient of electron density.

Kohn and Sham hypothesized a way to obtain the ground state electron density. According to the Kohn-Sham scheme, we need to solve a set of single electron wave functions that only depend on three spatial variables, $\psi(r)$.

$$\left[-\frac{\hbar^2}{2m}\nabla^2 + V(r) + V_H(r) + V_{XC}(r)\right]\psi_i(r) = \varepsilon_i(r)\psi_i \qquad (1.15)$$

The Hamiltonian of this single electron wave function consists of kinetic energy, external potential, Hartree potential due to electron interacting with electron density, and the exchange correlation potential which needs to be approximated.

In the self-consistent scheme, initially a trial electron density, n(r) is guessed. This trial electron density, n(r) is put into the Hamiltonian of equation (1.15). Solving this Kohn-Sham equation gives a single electron wave function $\psi_i(r)$. For each electron, the Kohn-Sham equation provides individual single electron wave functions. After evaluating the wave functions for all the electrons we can recalculate the electron density from equation (1.10). If this new electron density is same as the trial electron density, then we have self-consistency in our loop. The true ground state is thereby achieved. Otherwise, the newly obtained electron density is used as a new trial density and the iteration process continues.

1.3   Plane Wave DFT

In our DFT work, we used open source DFT package ABINIT. Like most of the commercially available DFT packages, ABINIT is also a plane wave DFT package. Our goal is to study various properties of nanoporous silicon manufactured from a single crystalline silicon by electrochemical etching process. A crystal is a periodic arrangement of atoms. Since we are dealing with a collection of atoms which is periodic in space, plane wave DFT package is particularly chosen. The positive charged nuclei in the atom is represented by a periodic potential, U(r) whereas free electrons are represented by plane waves, $e^{ik\cdot r}$ in a crystal. When a free electron is put in a crystal having a periodic potential, the wave function results in Bloch waves expressed as:

$$\psi_{nk}(r) = exp(ik \cdot r)u_{nk}(r) \qquad (1.16)$$

This Bloch wave is still plane wave in nature but modulated by the potential which is also periodic with the lattice. In general, it's kind of perturbed free electron. There are couple of important concepts in actual plane wave DFT calculations for use in any DFT package. Those concepts are depicted below:

1.3.1 Cutoff Energy

In any practical DFT calculation, a set of atoms needs to be specified. When this set is repeated in every direction, the full three dimensional crystal structure is generated. This can be achieved by defining a volume which fills space when replicated in all directions. Next, the coordinates of atoms are defined that lie within this volume. These volume and the atom coordinates collectively form a supercell. Supercell needs to be defined in the input file of the DFT package. This supercell is represented by a lattice vector comprising the real space. The Fourier transformation of the real space is defined as the reciprocal space. In general, all the dimensions in real space gets inside out in reciprocal space. The bigger quantities is real space becomes smaller in reciprocal space and vice versa. We know that any periodic function can be expanded by a Fourier series. In the Bloch function defined in equation (1.16), the right most parameter $u_{nk}(r)$ is periodic with lattice. This periodic function if expanded by Fourier series, becomes reciprocal lattice vector.

$$\psi_{nk}(r) = exp(ik \cdot r)u_{nk}(r) = exp(ik \cdot r)\sum_{G} c_k exp(iG \cdot r) \tag{1.17}$$

From the above equation we can say that the Bloch wave can be represented as the sum of plane waves. Each plane wave here has kinetic energy,

$$E = \frac{\hbar^2}{2m}|k + G|^2 \tag{1.18}$$

Here, the plane waves need to be summed over infinite number of reciprocal lattice vectors due to the fact that lattice vector in real space becomes infinite in reciprocal space. Kinetic energy of each of the plane waves also increase with the size of the

reciprocal lattice vector. Evaluating the sum of plane waves over this infinite reciprocal lattice vectors doesn't make sense. This makes the cutoff energy an important criteria in practical DFT calculations. While evaluating the sum of the plane waves, we discard the plane waves having higher kinetic energy than this cut off energy.

1.3.2   k-Points

The plane wave wavevectors span the reciprocal space. The primitive unit cell in this reciprocal space is called the 1st Brillouin Zone (BZ). Any wavevector, k that differs the primitive cell or the 1st Brillouin Zone by the reciprocal lattice vector G can be written as $k' = k + G$. This k' is actually a phase shifted version of the original wavevector k. Therefore, we consider the plane wave wavevectors inside the 1st Brillouin Zone that will be sufficient to capture the whole scenario. In other words, integrals need to be evaluated only in the 1st Brillouin Zone. Accordingly, appropriate number of k-points must to be chosen to sample the Brillouin Zone. Finally, the integrals are evaluated by summing up over these k-points. Number of k-points needs to be sufficiently large to sample the BZ and to get reliable energy.

1.3.3   Pseudopotential

Chemical bonding and other characteristics of materials are mainly dependent on outer shell electrons known as valence electrons. Electrons lying in the core are thus less important. To make DFT calculations easier, the electron density of these less important core electrons can be replaced by a smoothed density. This is known as frozen core approximation. The pseudopotentials approximate this core electrons as a net positive potential and replace the electron density by a smoothed density. Almost all the commercial DFT codes provide the library of pseudopotentials for a list of different elements.

1.3.4   Supercells and Periodic Boundary Conditions

While doing practical DFT calculation, we implement unit cell or the supercell as the most basic input. This unit cell or supercell is repeated periodically in all three dimensions for DFT calculations. Due to this replication, there will be interaction across the periodic boundaries. Simply, we need to specify a set of atoms inside a full three dimensional crystal structure. This can be done by specifying a volume and specifying the coordinates of a set of atoms inside this volume that will fill up the volume. When these volume is repeated in x, y, and z directions, it actually specifies the full three dimensional crystal structure in space. The vectors defining the cell volume and the atom coordinates comprise the supercell. If the supercell is defined using minimum number of atoms, it is called primitive cell.

1.4   Nanoporous Silicon Matrix

Silicon has a diamond cubic crystal structure with a lattice constant of 5.43 Å(Angstrom). Silicon crystal has a shape of a simple cube with each side length of 5.43 Å and consisting of two inter-penetrating face centered cubic primitive lattices. The conventional silicon unit cell consists of 8 atoms [6]. The atom coordinates that fill up the conventional unit cell volume is given in table 1.1.

In our nanoporous silicon matrix, 3.5nm pore diameter is considered based on experimental evidence. We would require a cube having sides exceeding 4nm along both x and y directions to allocate a complete pore. It will take at least 8 (0.543×8 nm>3.5 nm) unit cells in both x and y direction. But, the total number of silicon atoms will be quite high and it will take extensive computational time to converge the DFT calculations. So, we decided to proceed with quarter pore only due to symmetry. A silicon supercell consisting of $4 \times 4 \times 4$ conventional unit cells was constructed. In this supercell, there were 512 silicon atoms in total. The silicon supercell looked like figure 1.1. The blue balls represent silicon atoms.

Table 1.1.
Atom coordinates in Si conventional unit cell

X-coordinate(Å)	Y-coordinate(Å)	Z-coordinate(Å)
0.00000	0.00000	0.00000
0.00000	2.71535	2.71535
2.71535	0.00000	2.71535
2.71535	2.71535	0.00000
4.07302	4.07302	1.35768
4.07302	1.35768	4.07302
1.35768	4.07302	4.07302
1.35768	1.35768	1.35768
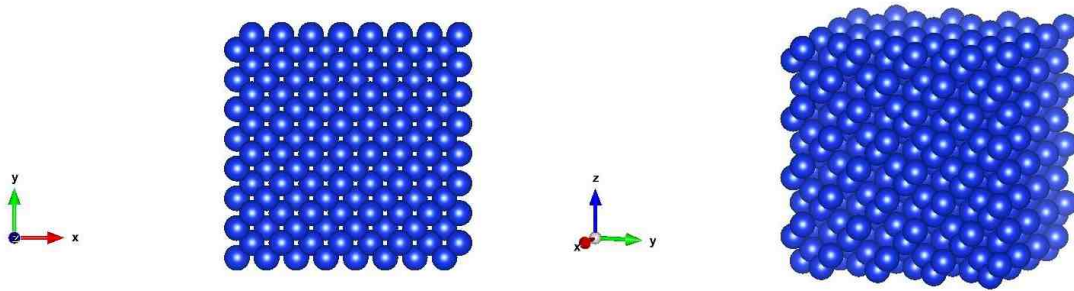
Fig. 1.1. $4 \times 4 \times 4$ Silicon supercell consisting of 4 conventional unit cells in x, y, and z directions: top view (left) and side view (right).

Next step was to remove some of the silicon atoms to place one quarter of the pore in our silicon supercell. The center of the pore was located at the top right corner of the supercell depicted in figure 1.1. A MATLAB function was written to remove the silicon atom coordinates lying within the pore radius of 1.75nm. Once this function was implemented, it etched away 172 silicon atoms from the system to imitate the

electrochemical etching procedure done in laboratory to produce nanoporous silicon. The pore depth was extended all the way to the bottom of the supercell. The pore was hexagonal in shape having edges along (100) and (110) planes.
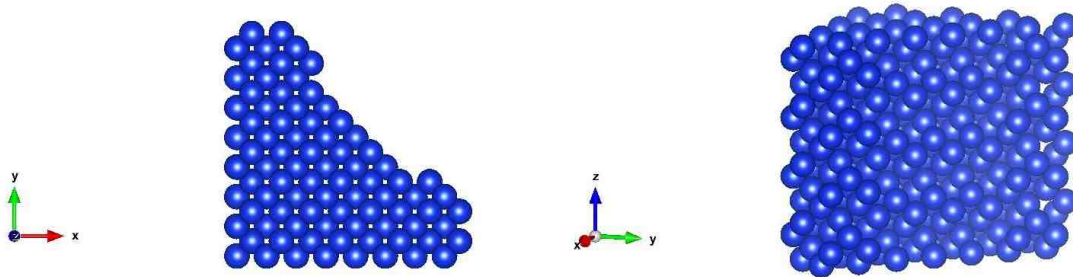
Fig. 1.2. Nanoporous silicon matrix accommodating one quarter of a pore in a $4 \times 4 \times 4$ silicon supercell: top view (left) and side view (right).

1.5 DFT Computational Setup: ABINIT

There are couple of commercial DFT packages available. Initially we started with the open source DFT package GAMESS [7]. GAMESS is an ab initio quantum chemistry code developed and maintained by Gordon research group at Iowa State University. We figured out couple of limitations of this package while working. For example: it doesn't support forming k-point grids essential to integrate over the 1st Brillouin Zone. Activating parallel computing in GAMESS is another painstaking task. But due to the nature of the size of our problem, parallel computation must be adopted. This is when we opted public licensed DFT tool ABINIT [8] to carry out our first principle DFT calculations. Throughout our DFT computation, LDA: new Teter (4/93) with spin-polarized option [9] was our choice of exchange-correlation functional and comes as default with ABINIT. This exchange-correlation functional

actually reproduces widely used Perdew-Wang functional. The choice of this default LDA exchange-correlation functional was justified by the fact that generalized gradient approximation (GGA) based exchange-correlation functionals are inferior in performance even though they utilize information about both local electron density and local gradient in electron density [10].

In our DFT code ABINIT, periodic boundary condition is applied in all three dimensions. This periodic boundary condition will create interaction between electron densities at the periodic boundaries. Since we intend to do surface study, it is required to use vacuum between two slabs of material [10]. The sufficient vacuum space between two slabs helps eliminating electron density in the vacuum. This essentially removes the impact of the top of one slab to the bottom of the slab above it. This vacuum space is generated by filling up the supercell partially along the z-dimension. The lower part of the supercell is filled with atoms whereas the upper part is kept empty. The atoms in lower part of the supercell fill the entire supercell in both x and y dimensions. When this supercell is periodically replicated in all three dimensions, they form stacked slabs of materials with a vacuum space between the slabs. These slabs are extended infinitely along x and y directions. Literature survey suggested a vacuum space of 15 Å (Angstrom) [11] to eliminate interaction between periodic images. Additional 4 unit cells (5.43 Å×4) are required to maintain a vacuum space of 15 Å. The supercell was expanded by another 4 conventional unit cells along z-dimension whereas x and y dimensions were kept same as before. This now becomes a $4 \times 4 \times 8$ silicon supercell. In this newly formed supercell, upper half was kept empty and only there were atoms in lower half of the supercell along z-direction.

The 1st Brillouin Zone was initially integrated by $2\times2\times2$ Monkhorst-Pack grid [12] before we introduced vacuum space between periodic images. Once the vacuum was introduced, the supercell dimension increased by a factor of 2 along z-dimension. Since dimension increase in real space corresponds to a decrease in reciprocal space, number of k-points along z-dimension needed to be reduced by a factor of 2. Therefore, 1st BZ was integrated by $2 \times 2 \times 1$ Monkhorst-Pack grid at the presence of vacuum.

Troullier-Martins pseudopotentials [13] were used for all the elements in our system including silicon, Pd, and hydrogen. Pseudopotentials of silicon and hydrogen were available with the DFT code, but the Pd pseudopotentials was retrieved from another DFT package, QuantumExpresso pseudopotential library [14]. A cutoff energy of 16 Ha (Hartree) was used for all the DFT computations done. 1 Ha is equivalent to approximately 27.21 eV. This results in a cutoff energy of 435 eV. A convergence study was carried out to choose the cutoff energy. We did a series of DFT computations for the cutoff energy ranging from 16 to 32 Ha with an increase of 4 Ha. The DFT calculations were pretty well converged with a maximum ground state total energy variance of 0.000001 eV. For higher values of cutoff energy, the DFT code needs to include more plane waves whose kinetic energy falls within this cutoff energy. Therefore, we chose 16 Ha as our cutoff energy. DFT is an iterative calculation where at the end of every iteration the newly evaluated electron density is compared to trial electron density. If those two electron densities match, the DFT code is said to have reached self-consistent solution. In reality, we are interested in finding the ground state total energy for a collection of atoms. Our DFT code reports the total energy corresponding to electron density at the end of each iteration. If the difference between two consecutive evaluations of total energy is less than tolerance value, the iterations are considered as converged. To make our DFT calculations highly precise, we chose a very low tolerance value of 0.000001 Ha.

1.6   KGB Parallelization

Due to high number of atoms in our nanoporous matrix we ported our DFT code to one of the biggest and fastest research supercomputing facilities of the world called Big Red II. Big Red II provides 1020 computing nodes, 21,824 processor cores, and 43,648 GB of RAM [15]. Since we had access to such huge computational resources, we wanted to activate parallel computing in ABINIT. The computational speed could be further increased by using KGB parallelization scheme. K, G, and B stands for

k-point, Wave vector of plane wave, and Band respectively. In KGB parallelization scheme, standard data partitioning was done over processors corresponding to k-points, block of bands, as well as Fourier space of coefficients over plane wave basis set [16]. As a result, three levels of parallelization can be achieved. This scheme gives us the provision to figure out the number of processors required on each level of parallelization [17]. KGB algorithm suggests suitable values for number of processors required for parallelization over k-point, plane wave wave vectors, and band level along with the projected efficiency. For each of our DFT calculations, we ran this KGB parallelization algorithm first to determine possible values of processors required for parallelization over these different levels. Suitable number of processors were chosen accordingly that corresponds to highest efficiency level.

2. METHODS

2.1 Catalyst

In as-synthesized nanoporous silicon (npSi) based hydrogen storage systems, complete dehydrogenation occurs at relatively high temperatures. At such high temperatures, silicon bond reformation takes place. Due to bond reformation, npSi looses suitability for further hydrogen recharge [3]. Nanoscale catalyst atoms play a very important role here in preventing bond reformation by bringing down the hydrogen desorption temperature and facilitating further hydrogen dissociation and spillover for gaseous recharge. Literature survey suggests various transition metals as suitable candidate as catalyst atom for hydrogen storage system. Transition metals are known for their contribution in H_2 dissociation into atomic hydrogen which later recombine with another atomic hydrogen to turn into molecular form and finally H_2 evolution between 300 and 900K [18]. The main challenge lies in overcoming the large activation barrier required to break the H-H bond. This H-H bond has a bond dissociation energy of 436 KJ/mol [19]. Among the transition metals, Pt and Pd are specifically known for their ability to reduce this substantial activation energy barrier [20] [21] and therefore facilitate H_2 dissociation. Strategic placement of catalyst atom is thereby a crucial factor in nanoporous silicon based hydrogen storage system. In npSi, Si-H and Si-H_2 are most prominent with a small number of Si-H_3 bonds [22]. In this Si-H_3 bonds, the silicon atom is bonded to only one neighboring silicon atom and is structurally the weakest among the three types of bonds silicon atoms form with hydrogen. During dehydrogenation, this structurally weak spots are supposed to give away hydrogen atom first. Green Fortress Engineering, Inc. holds a patent to strategically deposit catalyst atom to this structurally weak spots [23]. Pd is chosen as preferred catalyst due to its known inclination for silicon. In this catalyst deposition method,

storage media is initially heated to a temperature for partial dehydrogenation where Si-H_3 bonds give away two hydrogen atoms. The nanoporous silicon matrix is then cooled from this temperature and Pd catalyst atom is deposited in a solution [24].

2.1.1 Single Atom Catalyst

In order to comply with the catalyst deposition patent mentioned in previous section, we have evaluated 9 (nine) different locations as possible strategic location for single catalyst atom on and adjacent to the intersection of (100) and (110) planes at the pore edge. Catalyst atom was placed on or adjacent to the intersection of (100) and (110) planes at the pore opening, moved along the pore depth, and also moved to the silicon surface. The part of porous silicon matrix we chose for our micro-level study comprises only about one quarter of a pore. The pore is apparently hexagonal in shape. After carefully observing this nanoporous silicon matrix at our hand, it's evident that majority of the silicon dangling bonds where silicon atom is weakly bonded to the porous matrix exist in one of the three places: periphery of the pores near pore opening, pore walls along the pore depth, or adjacent to the pore edge on the top surface. Possible locations of single catalyst atom was chosen according to the symmetry of the pore morphology and presence of these dangling bonds. In all these locations, the silicon atom on which the catalyst atom is located is bonded to either one or two neighboring silicon atoms. Therefore, these are the structurally weak spots favorable for strategic deposition of catalyst atoms. The following figures show all 9 locations chosen as possible location of Pd catalyst atom for our DFT study. Blue balls represent silicon atoms in a nanoporous silicon matrix whereas silver balls represent Pd catalyst atoms deposited at strategic location. It is worth mentioning here that the (100) plane is along x-axis depicted in the figures and the (110) plane is along the diagonal of the porous matrix.

Fig. 2.1. Single Pd atom placed on a quarter pore of porous silicon along (110) plane at the pore mouth: top view (left) and side view (right).

Fig. 2.2. Single Pd atom placed on a quarter pore of porous silicon along (110) plane at pore depth: top view (left) and side view (right).

Fig. 2.3. Single Pd atom placed on a quarter pore of porous silicon adjacent to (110) plane on silicon surface: top view (left) and side view (right).

Fig. 2.4. Single Pd atom placed on a quarter pore of porous silicon at the intersection of (100) and (110) plane at the pore mouth: top view (left) and side view (right).
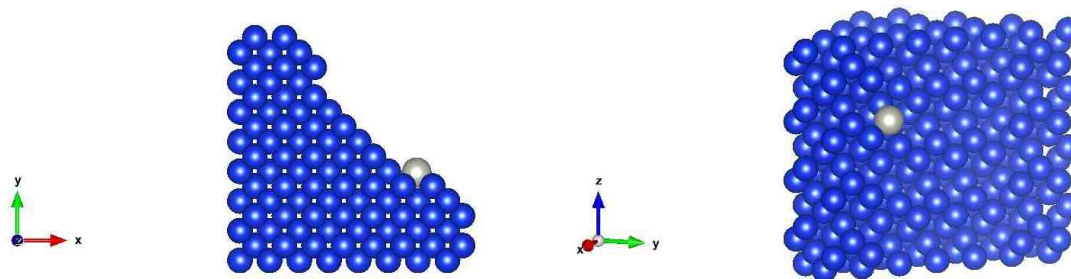
Fig. 2.5. Single Pd atom placed on a quarter pore of porous silicon at the intersection of (100) and (110) plane at the pore depth: top view (left) and side view (right).
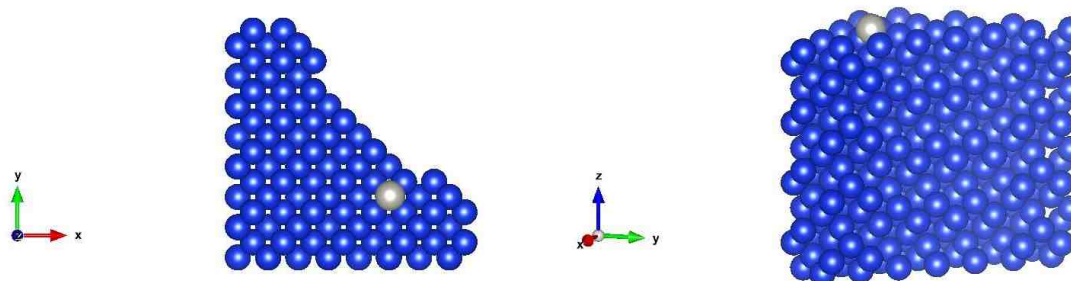
Fig. 2.6. Single Pd atom placed on a quarter pore of porous silicon adjacent to the intersection of (100) and (110) plane on silicon surface: top view (left) and side view (right).

In nature, any collection of atoms always tend to go to lowest energy state. This lowest energy state is most stable quantum state for the collection of atoms. In our single catalyst atom study, we calculated the ground state total energy using our DFT package for the collection of 340 silicon atoms and 1 Pd catalyst atom. The silicon atoms are kept fixed whereas the Pd atom is moved to all the 9 locations we
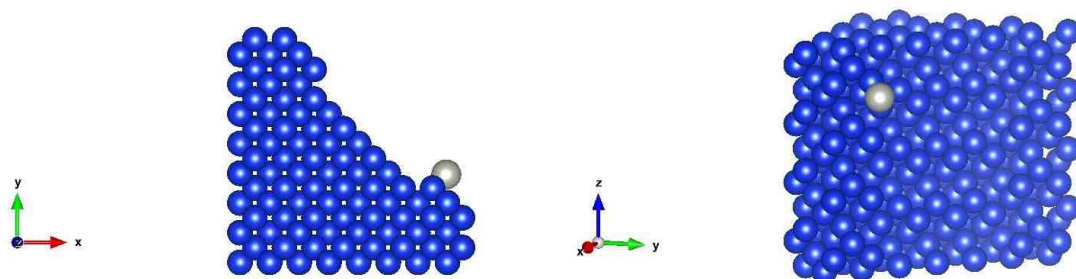
Fig. 2.7. Single Pd atom placed on a quarter pore of porous silicon along (100) plane near pore mouth: top view (left) and side view (right).
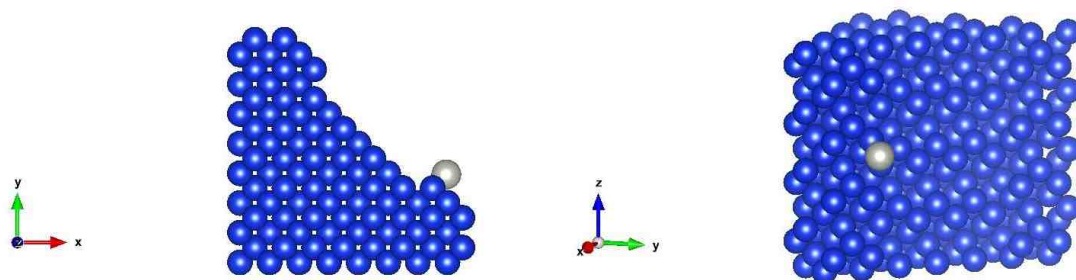
Fig. 2.8. Single Pd atom placed on a quarter pore of porous silicon along (100) plane at the pore depth: top view (left) and side view (right).

investigated. The ground state total energies for all the 9 locations are then compared. Naturally, the one with lowest ground state energy denotes the most stable quantum state and therefore most favorable location for Pd atom.
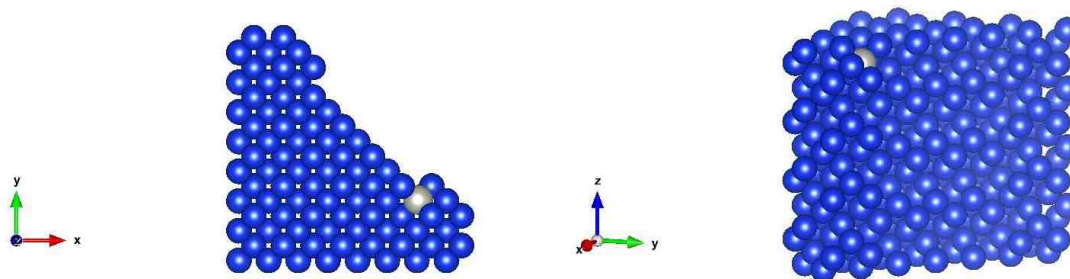
Fig. 2.9. Single Pd atom placed on a quarter pore of porous silicon adjacent to (100) plane on silicon surface: top view (left) and side view (right).

2.1.2   Multiple Atom Catalyst

Catalyst atoms are expected to form clusters of at least 2 (two) or more atoms to facilitate gaseous hydrogen dissociation and spillover process [25]. To ensure high energy density storage media where almost all the dangling silicon bonds are terminated by hydrogen atoms for complete hydrogenation, spillover process must take place. For spillover process to happen, the chemical potential of hydrogen needs to be increased to a spillover favorable range [26]. Single Pd atom may not be enough to dissociate required number of gaseous H_2 to raise the H chemical potential to a range required for spillover. Therefore, we need to consider clusters consisting of multiple catalyst atoms. As the size of the cluster increases, multiple H_2 molecules are adsorbed to the cluster [27] [28]. These H_2 molecules are dissociated and increases the H chemical potential to a spillover favorable range. For palladium, the tetrahedron structure consisting of 4 (four) atoms is found to be lowest in energy in DFT study [26] and are most stable. Therefore, we have considered this tetrahedron structure of catalyst atoms and evaluated at three different locations as possible strategic location for catalysis. The reason behind the choice of these 3 locations were similar to the case as single catalyst atoms where the main consideration for possible strategic lo-

cation of catalyst atom was the structurally weak spots having lesser number of Si-Si bonds. Catalyst structures were placed on and adjacent to the intersection of (100) and (110) planes at the pore edge near the pore opening. Different orientations of the tetrahedron structure is also considered which will be discussed in detail in later sections.
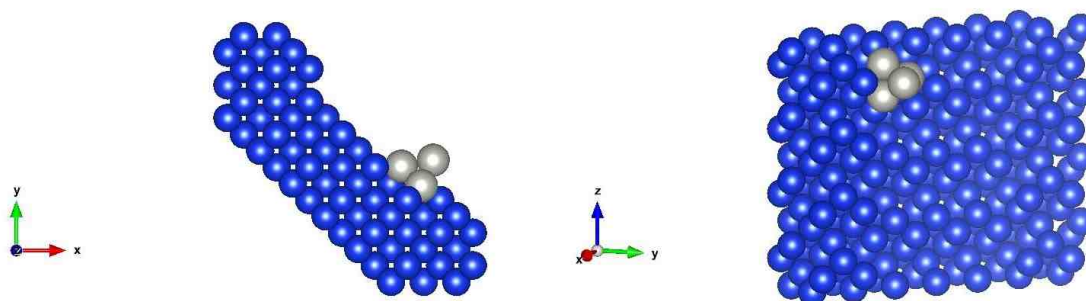
Fig. 2.10. Cluster of 4 Pd atoms placed on a quarter pore of porous silicon adjacent to the intersection of (100) and (110) plane: top view (left) and side view (right).
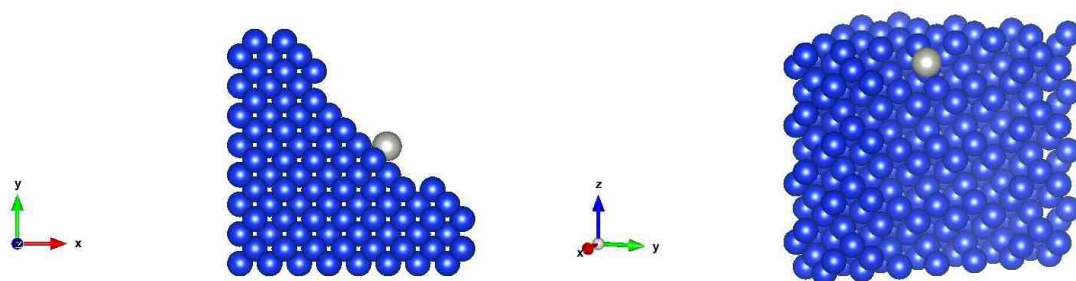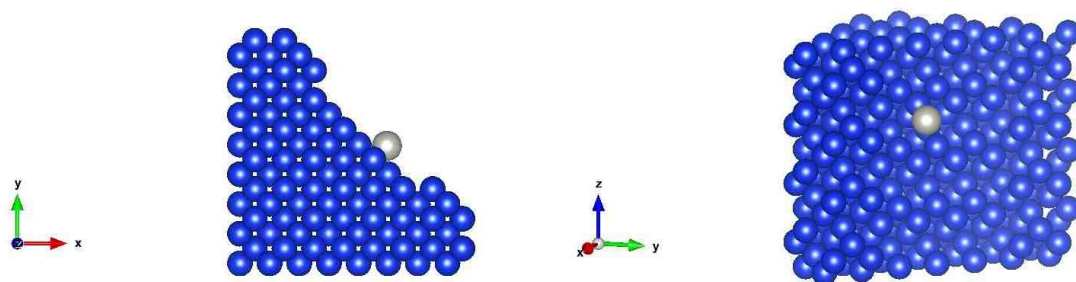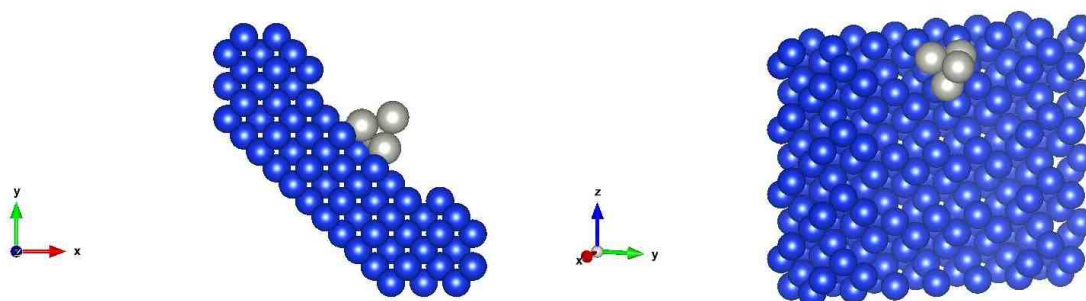

Fig. 2.11. Cluster of 4 Pd atoms placed on a quarter pore of porous silicon along (110) plane: top view (left) and side view (right).
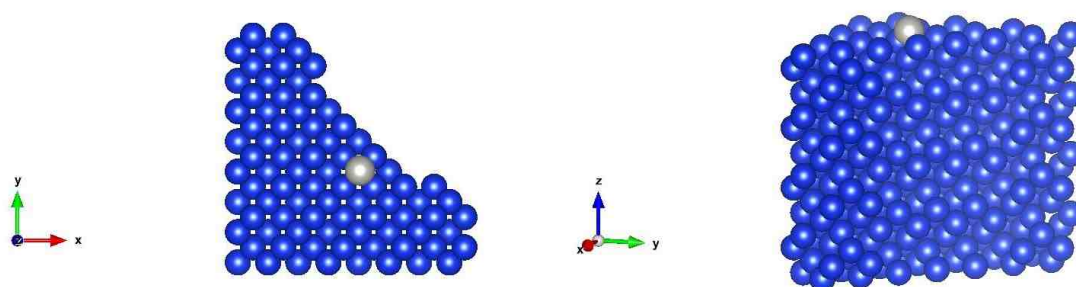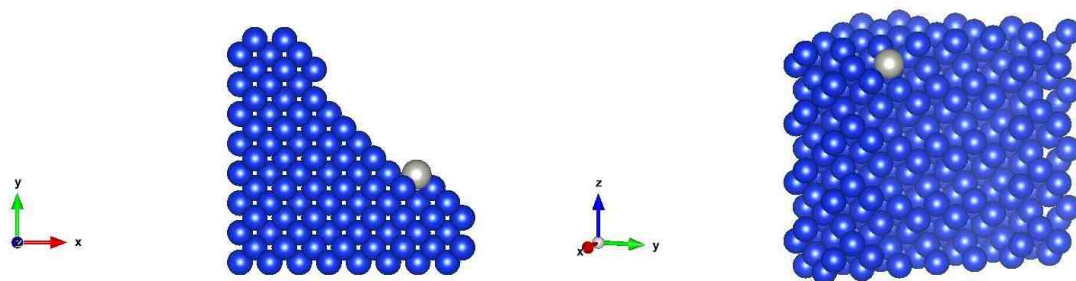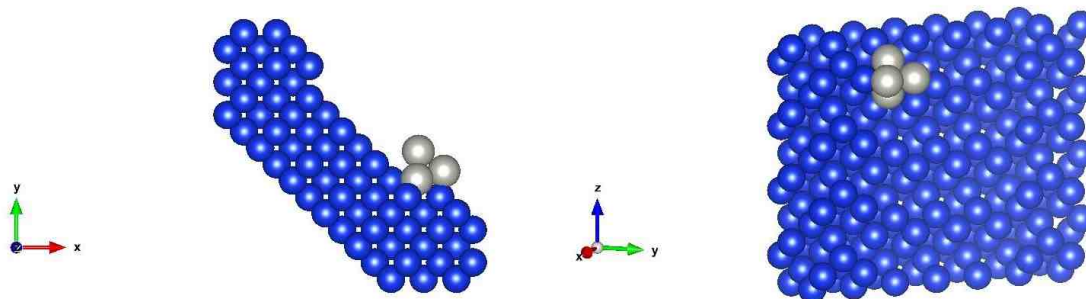
Fig. 2.12. Cluster of 4 Pd atoms placed on a quarter pore of porous silicon at the intersection of (100) and (110) plane: top view (left) and side view (right).

With the increasing size of the catalyst cluster, total number of atoms in the system was increasing. In DFT packages, the computational effort increases substantially with the size of the system. In our micro-scale system, there were 344 atoms in total. Even though we were doing our DFT computations in one of the fastest research supercomputer facilities of the world, the computational time was extensive. For the collection of 340 silicon atoms and Pd cluster consisting of 4 Pd atoms, we ran the computation in Big Red 2 with an actual elapsed time of 48 hours. In high performance computing jargon, this difference between actual program start time and end time for any computational job is called "wall time". During this 48 hours of wall time, the computation was running in 288 processors in parallel for our job. Thus, the CPU time was much higher than the wall time. The ground state energy didn't converge within the specified wall time. The DFT package provides several output files (ie: density file, wave function file, etc.) at the expiration of the wall time. We were able to utilize the density file to restart the computation from right where it stopped which actually provides the latest trial density used by the DFT package in pursuit of finding ground state electron density. Even after several restarts and an approximate computational time of around 2 weeks, the job didn't converge. That's

when we realized, our micro-scale system was too large for the DFT package to handle. We needed to minimize computational effort by reducing the size of the system in a way that the morphology, shape, and characteristics of the system as well as the individual property of the bulk silicon and catalyst atoms are preserved. Therefore, silicon atoms that fall beyond the range of 4 (four) atoms in any direction except for the z-direction were discarded. The new system had substantially fewer number of atoms while the pore morphology, shape, and properties were preserved.

2.2   Dissociation

The main role of catalyst atoms in our system is to facilitate the dissociation of gaseous H_2 to atomic hydrogen so that it can subsequently spillover onto the silicon surface, as explained in the next subsection. Hydrogen is finally stored in solid state in this silicon surface. We have studied hydrogen dissociation for both single catalyst atom and tetrahedron catalyst structure. Since we are interested in studying dissociation of gaseous H_2 on Pd catalyst supported at silicon surface, we defined the supercell in such a way that there were vacuums along part of the z-coordinates as described in previous sections. One gaseous H_2 was placed 15 Å(Angstrom) away from the surface right above the pore whereas the single catalyst atom or tetrahedron catalyst cluster was supported on the silicon surface at the lowest energy location. H_2 was placed in vacuum at a position where it doesn't overlap with the silicon atoms to ensure sufficient separation between periodic images [11]. This helps in achieving easier plane wave solution. Due to the presence of a metal atom in the system, macroscopic dielectric constant value was raised and this new value was used onwards for speeding up the Self Consistent Field (SCF) procedure. Like the catalyst study mentioned in previous section, reduced number of silicon atoms were considered in case of tetrahedron catalyst structure. The dissociation energy barrier is calculated

by comparing the total energy of the silicon substrate with one molecule of hydrogen present 15 Å away in gaseous state with the energy of silicon substrate while the molecular hydrogen gets dissociated and forms two bonds with catalyst atom(s).
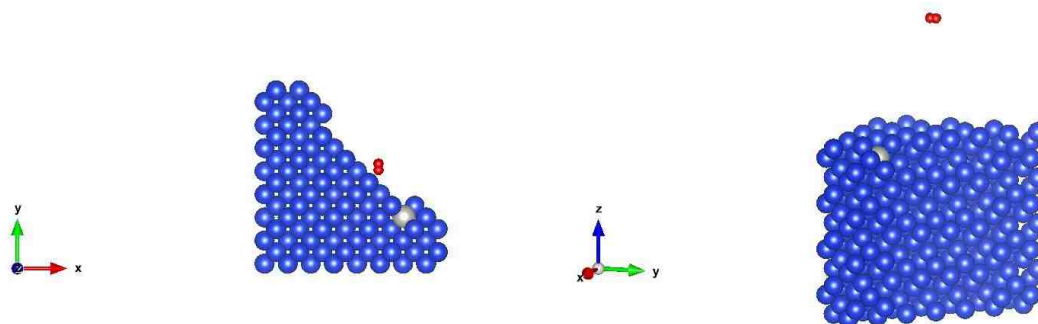
Fig. 2.13. Gaseous H_2 molecule placed on top of pore 15 Å away from surface containing single Pd catalyst: top view (left) and side view (right).
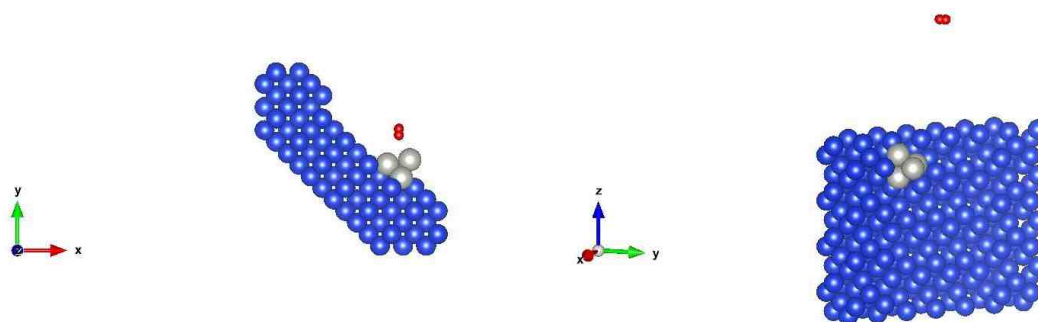
Fig. 2.14. Gaseous H_2 molecule placed on top of pore 15 Å away from surface containing Pd cluster consisting of 4 Pd atoms: top view (left) and side view (right).

2.3   Spillover

Spillover is the pathway through which hydrogen atoms move from the catalyst atoms supported at the silicon substrate to the nearby silicon surface. Hydrogen uptake in a storage medium is significantly increased by spillover from a supported heterogeneous metal catalyst [25] [29]. It is assumed that the hydrogen atoms find their way in the nearby low valence silicon surface atoms after spillover process. Therefore, nearby silicon atoms having valence value of 2(two) or 3(three) are the probable sites for hydrogen termination after spillover process. In this thesis, we have carried out spillover study for both single catalyst atom and tetrahedron catalyst structure. The spillover energy barrier is calculated by comparing the total ground state energy of the silicon substrate along with dissociated hydrogen atoms forming bonds with catalyst atom(s) to the energy of silicon substrate supporting catalyst atom(s) with two adjacent low valence silicon atoms terminated by hydrogen atoms.
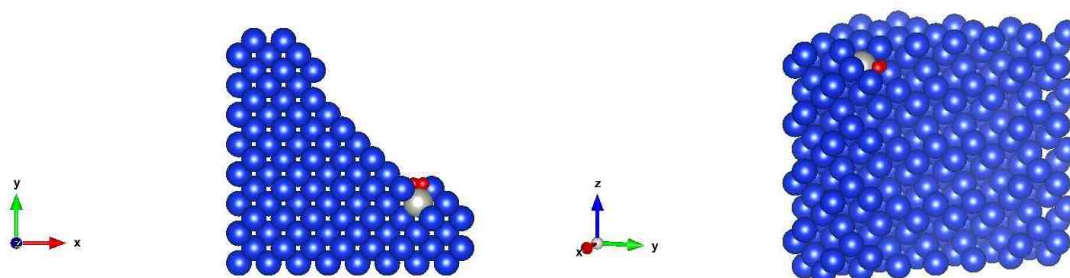
Fig. 2.15. Before Spillover: atomic hydrogen forms bond with Pd catalyst; top view (left) and side view (right).
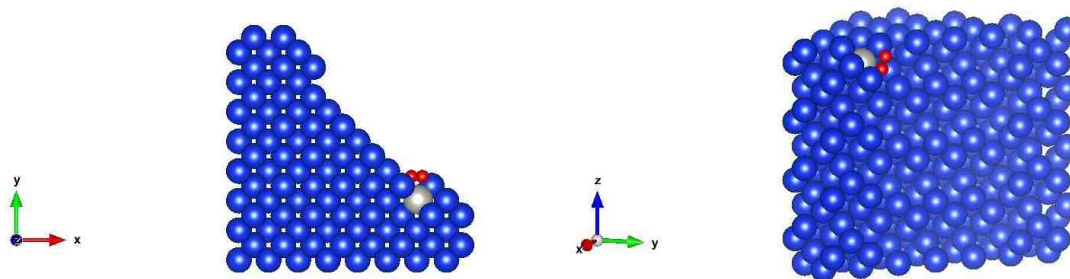
Fig. 2.16. After Spillover: split hydrogen forms bond with low valence silicon at nearby surface; top view (left) and side view (right).

2.4 Recharge-Discharge State

Ground state total energy at fully recharged and completely discharged porous silicon matrix was calculated using ABINIT. The difference between these two quantities provide the the energy required for recharging the porous silicon matrix. With 1(one) Pd catalyst atom near pore edge at the one quarter of the pore, every silicon atom located in top surface and pore wall having less than 4 nearest neighbor silicon atoms was terminated by hydrogen atoms in solid state. The number of nearest neighbor atoms from any silicon atom in silicon crystal is defined as the coordination number of silicon. When all these mentioned silicon atoms having coordination number less than 4 were terminated by hydrogen atoms, this represents fully charged state. The system looked like figure 2.17 at recharged state.

On the other hand, exact same number of atomic hydrogens (ie: 102 atoms) but in molecular gaseous form (ie: 51 gaseous H_2) were uniformly distributed in the vacuum space over the pore. We needed a bigger supercell to accommodate these 51 gaseous H_2 molecules in the vacuum space. Therefore, we extended the supercell along z-direction only. A new $4 \times 4 \times 15$ supercell was constructed. Gaseous H_2 molecules
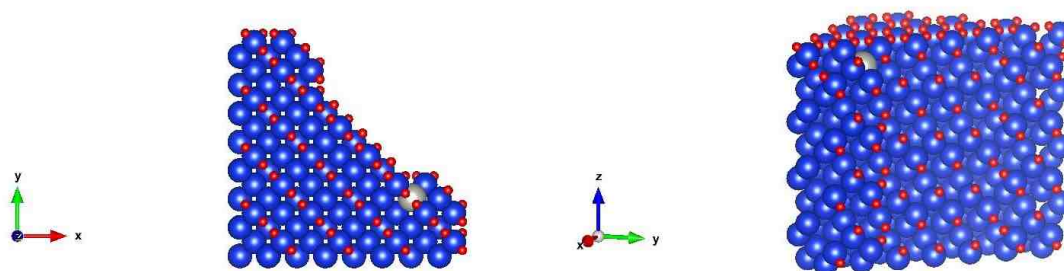
Fig. 2.17. Complete Recharged Porous Silicon Matrix at Solid State:
top view (left) and side view (right).

were uniformly distributed in the vacuum space ensuring a minimum of 15 Å distance
between the top of silicon surface and the gaseous hydrogen molecule closest to this
silicon surface. This represents the completely discharged state. The system looks
like figure 2.18 at discharged state.
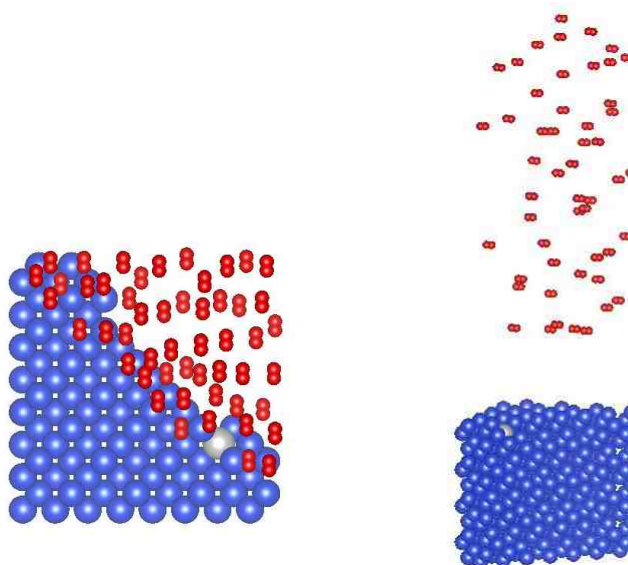
Fig. 2.18. Complete Discharged Porous Silicon Matrix: Gaseous H_2
in Vacuum Space: top view (left) and side view (right).

Like we mentioned in section 2.2, we tried to place the H_2 molecules in a way that none of them are located on top of silicon to ensure easier plane wave solution for this configuration. But still we ended up placing few H_2 molecules on top of silicon because of limited dimension in real space. Forcing all the H_2 molecules close together will imply high pressure in our system. In order to avoid that, we moved some of the H_2 molecules on top of silicon to ease off this situation.

Apart from studying the energy difference between fully charged and fully discharged state only, some intermediate steps were also created in a step size of 25 percent where in each successive step 25 percent more hydrogen atoms were loaded on silicon surface in solid state. Rest of the hydrogens remain in gaseous state as H_2 molecule. In all the cases, total number of hydrogen atoms in the system were same. The ground state total energy was calculated for all these configurations. A random number generator function was used to remove the gaseous hydrogen molecules and load them on silicon surface or inside the pore. In total six different random samples were taken for this analysis. The system looked like following in different hydrogen loading states:
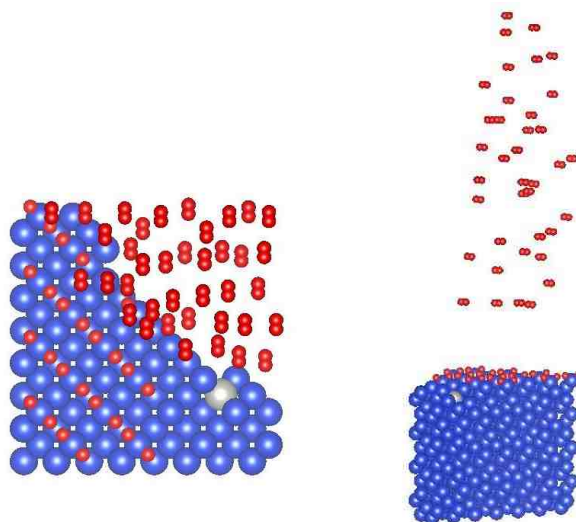
Fig. 2.19. 25% Recharged Porous Silicon Matrix: 38 numbers of gaseous H_2 in Vacuum Space whereas 26 numbers of H atom in silicon surface at solid state; top view (left) and side view (right).
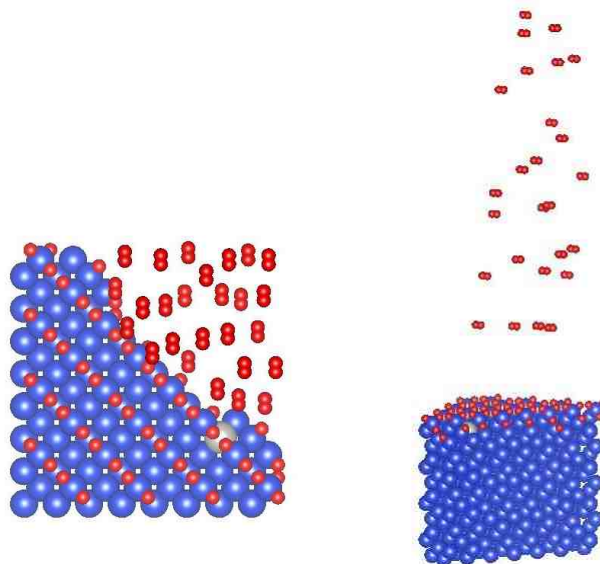
Fig. 2.20. 50% Recharged Porous Silicon Matrix: 26 numbers of gaseous H_2 in Vacuum Space whereas 50 numbers of H atom in silicon surface at solid state; top view (left) and side view (right).
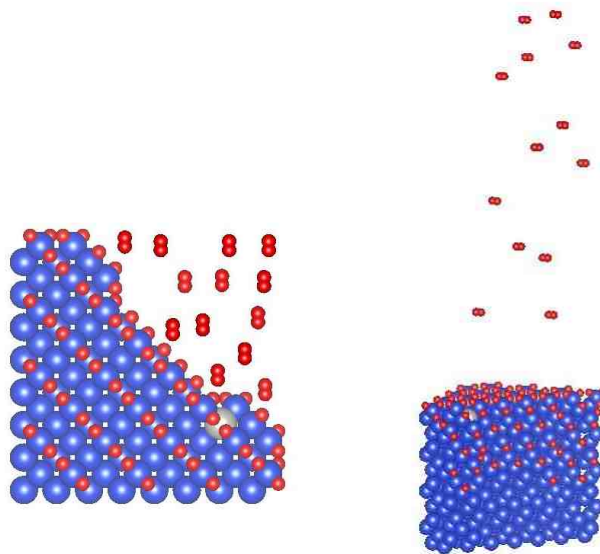
Fig. 2.21. 75% Recharged Porous Silicon Matrix: 13 numbers of gaseous H_2 in Vacuum Space whereas 76 numbers of H atom in silicon surface at solid state; top view (left) and side view (right).

2.5 Bond hopping

After spillover process, bond hopping process is initiated. In the bond hopping process, the hydrogen atoms terminated in surface silicon atoms hop to the next available silicon atoms which are 1 (one) atom further moved down the adjacent silicon unit cell along z-direction. Therefore, initially we hypothesized of a bond hopping distance of 5.43 Å. We initiated our bond hopping study by considering bond hopping along z direction only. Catalyst atom(s) was removed since bond hopping occurs far away from catalyst atom(s) and thereby catalyst has negligible or no impact.
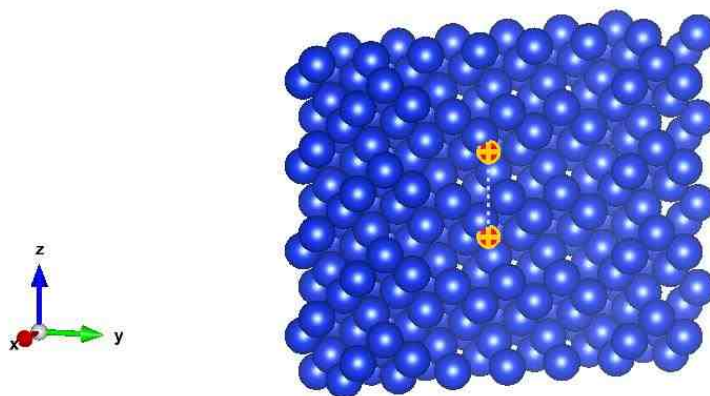
Fig. 2.22. Bond Hopping Along Z-direction only with a Hopping Distance of 5.43 Å.

We kept the hydrogen atom fixed at the initial and final locations and then took 9 (nine) equidistant intermediate points in a straight line along z-direction. In total there were 11 (eleven) points including the initial and final positions. We call this images. We calculated ground state total energy for all those 11 images using DFT. When the difference in ground state total energy was plotted against the hopping distance in MATLAB, we got following graph:
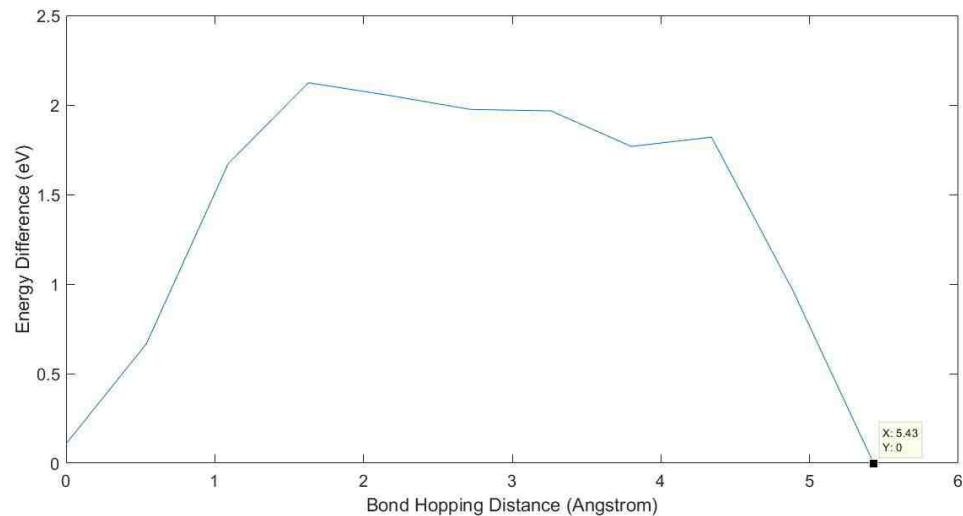
Fig. 2.23. Energy difference (eV) vs Bond Hopping Distance (Å) for bond hopping in a straight line along z-direction.

The above figure demonstrates two local minima separated by a transition state. The transition state is located around 1.63 Å away from the initial state where hydrogen atom is bonded to the surface silicon atom. The ground state energy of the transition state gave an energy barrier of 2.12 eV hydrogen atom has to overcome in order to bond hop to the next silicon atom. In reality, this is highly unlikely that the hydrogen atom will have no movement along x and y-directions and will bond hop along a straight line. Therefore, we decided to manually move the hydrogen atom along x and y directions within a radius of 0.10 Å while the z-coordinate was kept fixed. We formed a cloud of possible locations for hydrogen atom. Hydrogen atom may exist in any of this locations during bond hopping. Our formed cloud consisted of around 120 points which is pretty extensive considering the wall time it took in Big Red II supercomputer. Roughly 10 points were considered for each of the images we considered in our previous study. Ground state total energy was computed for all those 120 positions. In figure 2.24, we have plotted the 3D cloud consisting of all the 120 manually created possible location of H atom in bond hopping pathway.

The size of the points increase with the increasing size of corresponding ground state energy. Therefore, it is likely that the bond hopping pathway will go through the string connecting the circle with smaller radius.
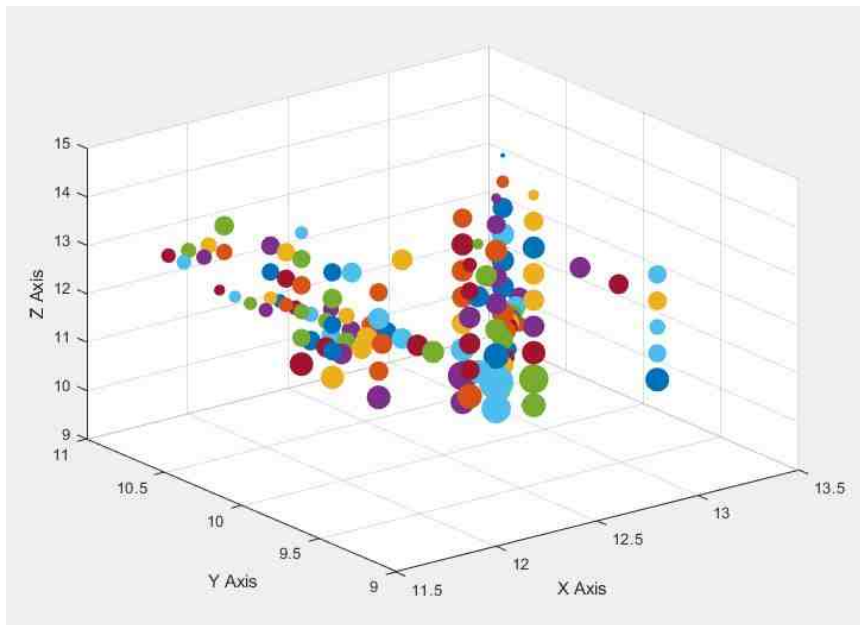
Fig. 2.24. 3D cloud of manually created possible location of H atom in bond hopping pathway

Next, we compared the ground state energy of all the points taken against any image and took the point with lowest energy. This process was repeated for all the 11 images. Thus, we took the minimum energy for all the 11 images and plotted the ground state total energy vs bond hopping distance in MATLAB. The graph looked like figure 2.25.

We figured out one additional local minima from this plot. Even though the bond hopping energy barrier got reduced significantly from 2.12 eV to around 1.54 eV, we can't assure that our study covers the actual bond hopping pathway since all the images were considered manually. But we got an important insight from this study. Presence of an additional local minima refers to the possibility of a quasi stable state between our initial and final image. Since there exist a high energy barrier between
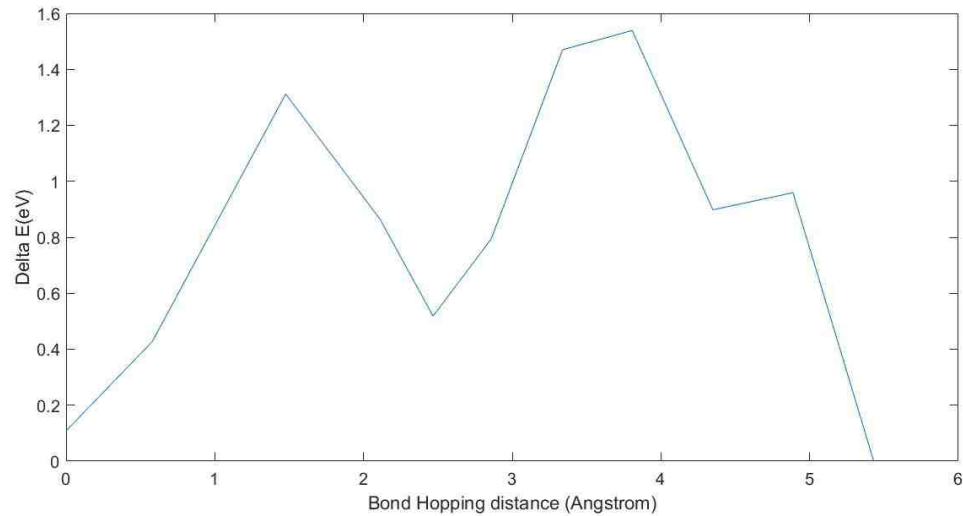
Fig. 2.25. Energy difference (eV) vs Bond Hopping Distance (Å) calculated by taking minimum energy values for each point along H atom's bond hopping pathway from a cloud of manually created points in a 3D space.

these two images, the hydrogen atom may complete one complete hop in two distinct steps having lower energy barrier. It may hop from initial state to this quasi stable state and finally the second hop from this state to final state will follow. The first hop was at distance of around 2.50 Å in a diagonal direction along the crystal face, the second hop had a distance of 2.93 Å. Thus, covering a total bond hopping distance of 5.43 Å.

2.5.1   String Method

Next, we wanted to find the bond hopping pathway using well established methods instead of creating images manually. We started off with *String Method*. The string method is a specialized algorithm that is widely used to find Minimum Energy Path (MEP) between initial and a final state [30]. ABINIT implements *Simplified String*

Method [31] where intermediate images are generated between initial and final images by linear interpolation method. A string connects the images. These intermediate images are elastic in nature. At the end of each iteration, they are moved in the direction of the forces acting on images and they get redistributed along the string connecting them. An equal distance between the images are maintained during this redistribution process. Thus, the string is slowly driven towards the minimum energy path after each iteration. At the end of each iteration, the ground state total energy is reported for each of the intermediate images. Once the difference of absolute energy between these images fall below the tolerance value, convergence is reached and the string connecting the images forms the minimum energy path [32].

We initiated the simplified string method by allowing the hydrogen atom to relax at the initial and final configurations. Once we relax the hydrogen atom, the forces acting on this atom is minimized. As a result, this configuration goes to its lowest energy state. This will ensure two local minima at the two ends of the string connecting the images. Relaxed Si-H had a bond length of 1.50 Å. ABINIT code was utilized to generate 11 intermediate images between this initial and final state. We used a tolerance value of 0.00001 Ha. Image parallelization on top of existing KGB parallelization scheme was used to distribute image level work-loads over a number of processors. We scheduled DFT computation jobs in ABINIT for both the parallel bond hopping paths:

i) Direct hop from initial to final state (Hopping Distance: 5.43 Å),

ii) Bond hop from initial to final state in two steps: first hop from initial to quasi stable state located diagonally along the crystal face and then second hop from there to final state. After Si-Pd bond relaxation, the first and second hopping distance turned out to be 2.90 and 3.75 Å respectively.

Unfortunately, the computation jobs didn't converge even after a computation time of 2 weeks in Big Red II. Therefore, we discarded this method and started to look for alternate methods.
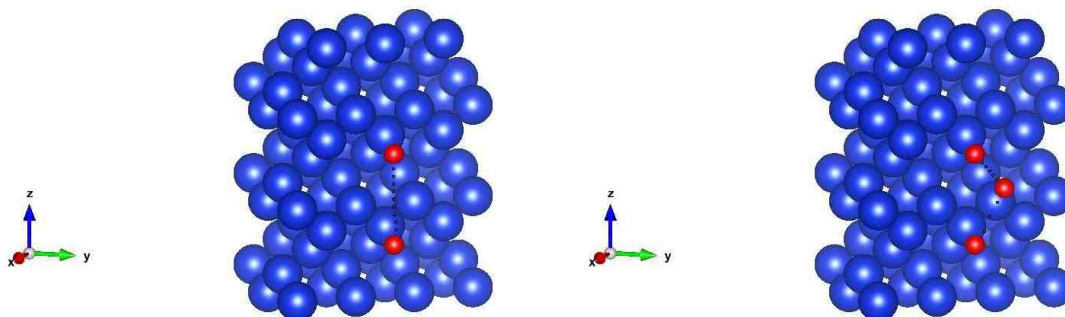
Fig. 2.26. Bond Hopping Alternate Pathways Consisting of Single Hop(left) and Double Hop(right).

2.5.2 Nudged Elastic Band (NEB) Method

From our string method study in finding minimum energy path, we assumed perhaps the tolerance value was pretty high. In fact, used tolerance value was 1000 times lower than default tolerance values in commercial DFT codes. Total number of atoms in the system was 242 which was also pretty high for plane wave solution to converge. This time number of atoms were further reduced to 85 and default tolerance value of 0.0001 Ha was used. From literature survey we figured a convergence to a minimum energy path is guaranteed in Nudged Elastic Band (NEB) method if enough number of images are considered [33].

ABINIT supports three distinct NEB methods: Original NEB method, Improved Tangent NEB method, and Climbing-Image NEB (CI-NEB) method. Due to the fact that this Climbing-Image NEB method initiates with several iterations of original NEB method, it's much more computing intensive [34]. So, we adopted the Improved Tangent NEB method in our transition state investigation. In this method, a spring connects the images. This spring has a spring constant associated. We used the ABINIT default value for the string constant. This default value is $2*0.05$ Ha/$bohr^2$. Just like the string method, linear interpolation method is used to generate equidistant

images between initial and final configurations. The resulting force acting on the images come from a combination of two forces. First, this particular configuration has its own potential energy surface. Second, the closest two configurations from the current configuration has a spring force acting upon it. The image needs to be changed according to this resulting force. The image is moved in such a way that the true force projects toward the direction perpendicular to the minimum energy path while the spring force from nearest neighboring configurations project parallel to the minimum energy path [35]. Thus at the end of each iteration, these images are moved. All these images connected together forms an energy path. When the tolerance convergence criteria is met, the energy path connecting the images is supposed to have coincided with the minimum energy path.

We considered both the bond hopping pathways mentioned in previous section. For alternate pathway consisting of two hops, the hydrogen atoms are located at a distance of 4.50 Å between which the first hop takes place. For the second hop, the distance is 2.35 Å. Therefore, we took 7 intermediate images for the first hop and 3 intermediate images excluding the initial and final configuration for second hop. For direct hop, total number of images were kept same as before. With this new method and new values of some of the input parameters, we reached the MEP convergence after restarting the computation from the density files reasonable amount of times. The restart from previous density file actually provides the new computation an educated guess of the possible minimum energy pathway that helps to reach the convergence.

2.6   Diffusion

There are two available parallel paths for hydrogen diffusion in porous silicon: diffusion through pores and diffusion carried out in a bond hopping process along silicon surface. Diffusion through the porous silicon matrix itself is slow enough to be negligible [36]. Pore diffusion can be derived analytically whereas hydrogen diffusion

along silicon surface needs to be investigated via density functional theory (DFT) study. Associated vibrational frequency modes needs to be calculated in order to figure out the hydrogen diffusion rate on porous silicon.

Since in our case the hydrogen atom is considered to be vibrating on silicon surface, the interaction between hydrogen atom and silicon atoms may impact the associated vibrational modes. Let us consider N atoms in the system and their cartesian coordinates are defined as a single vector, r = $(r_1,....,r_{3N})$. Here, r consists of 3N components. We further consider the local energy minima is located at r_0. New coordinate is defined as $x = r\text{-}r_0$. Next, we take the Taylor expansion along the energy minima at r_0 ignoring terms with order greater than 2. This approach of ignoring higher order terms is known as harmonic approximation [10].

$$E = E_0 + \frac{1}{2} \sum_{i=1}^{3N} \sum_{j=1}^{3N} \left[\frac{\partial^2 E}{\partial x_i \partial x_j} \right]_{x=0} x_i x_j \tag{2.1}$$

The first derivative term in Taylor expansion is zero because it was evaluated at energy minima. Let us define a Hessian matrix consisting of $3N \times 3N$ elements defined by,

$$H_{ij} = \left[\frac{\partial^2 E}{\partial x_i \partial x_j} \right]_{x=0} \tag{2.2}$$

If we define the atoms as classical particles following Newton's law of motion, then we will have, $F_i = m_i \ (d^2 x_i/dt^2)$. Here, the force and mass associated with ith coordinate are F_i and m_i respectively and $(d^2 x_i/dt^2)$ is the acceleration of this coordinate. If we rewrite the equation of motion in matrix form,

$$\frac{d^2 \mathbf{x}}{dt^2} = -\mathbf{A}\mathbf{x}$$

This is the mass-weighted Hessian matrix whose elements are defined as, $A_{ij} = H_{ij}/m_i$. This matrix form equation have special set of solutions associated with the eigenvectors of $\mathbf{A}$. These special solutions are called the normal modes. The eigenvector of this matrix and their eigenvalues satisfy following equation,

$$\mathbf{A}\mathbf{e} = \lambda \mathbf{e}$$

Here, λ and $\mathbf{e}$ are eigenvalues and eigenvectors of matrix $\mathbf{A}$ respectively. At initial condition (t=0), the motion of all the atoms is given by x(t=0)=a$\mathbf{e}$ and $d\mathbf{x}$(t=0)/dt=0, then the position of atoms can be defined in following form:

$$\mathbf{x}(t) = a cos(\omega t)\mathbf{e} \tag{2.3}$$

Here, a is an arbitrary constant and $\omega = \sqrt{\lambda}$. In general, $\mathbf{A}$ has 3N eigen vectors and corresponding eigenvalues. The 3N normal mode frequencies then can be defined using the 3N eigenvalues as follows,

$$\nu_i = \frac{\sqrt{\lambda_i}}{2\pi} \tag{2.4}$$

Now, the bond hopping frequency calculation of hydrogen atom will result in 3N = 3 eigenvalues due to the fact that hydrogen atom has 3 (three) degrees of freedom along three spatial coordinates. The Hessian matrix in our case will be a 3x3 matrix defined as follows:

$$H_{ij} = \begin{pmatrix} \frac{\delta^2 E}{\delta x^2} & \frac{\delta^2 E}{\delta x \delta y} & \frac{\delta^2 E}{\delta x \delta z} \\ \frac{\delta^2 E}{\delta y \delta x} & \frac{\delta^2 E}{\delta y^2} & \frac{\delta^2 E}{\delta y \delta z} \\ \frac{\delta^2 E}{\delta z \delta x} & \frac{\delta^2 E}{\delta z \delta y} & \frac{\delta^2 E}{\delta z^2} \end{pmatrix} \tag{2.5}$$

Now, from finite difference approximation the diagonal elements of the Hessian matrix are defined as,

$$\frac{\delta^2 E}{\delta x^2} \approx \frac{E(x + \delta x, y, z) - 2E(x, y, z) + E(x - \delta x, y, z)}{\delta x^2}; \tag{2.6}$$

$$\frac{\delta^2 E}{\delta y^2} \approx \frac{E(x, y + \delta y, z) - 2E(x, y, z) + E(x, y - \delta y, z)}{\delta x^2}; \tag{2.7}$$

$$\frac{\delta^2 E}{\delta z^2} \approx \frac{E(x, y, z + \delta z) - 2E(x, y, z) + E(x, y, z - \delta z)}{\delta z^2}; \tag{2.8}$$

However, the non-diagonal elements are defined as following according to finite difference approximation:

$$\frac{\delta^2 E}{\delta x \delta y} \approx \frac{E(x + \delta x, y + \delta y, z) - E(x + \delta x, y - \delta y, z) - E(x - \delta x, y + \delta y, z) + E(x - \delta x, y - \delta y, z)}{4\delta x \delta y};$$

$$\tag{2.9}$$

$$\frac{\delta^2 E}{\delta y \delta z} \approx \frac{E(x, y + \delta y, z + \delta z) - E(x, y + \delta y, z - \delta z) - E(x, y - \delta y, z + \delta z) + E(x, y - \delta y, z - \delta z)}{4 \delta y \delta z};$$
$$(2.10)$$

$$\frac{\delta^2 E}{\delta z \delta x} \approx \frac{E(x + \delta x, y, z + \delta z) - E(x - \delta x, y, z + \delta z) - E(x + \delta x, y, z - \delta z) + E(x - \delta x, y, z - \delta z)}{4 \delta z \delta x};$$
$$(2.11)$$

Due to symmetry,

$$\frac{\delta^2 E}{\delta x \delta y} = \frac{\delta^2 E}{\delta y \delta x}; \qquad (2.12)$$

$$\frac{\delta^2 E}{\delta y \delta z} = \frac{\delta^2 E}{\delta z \delta y}; \qquad (2.13)$$

$$\frac{\delta^2 E}{\delta z \delta x} = \frac{\delta^2 E}{\delta x \delta z}; \qquad (2.14)$$

But since the H atom orientation is along the (110) plane, we need to rotate the x and y axis by an angle of 45 degrees. A simple rotation matrix is used to serve the purpose. The rotation matrix is defined as:

$$R = \begin{pmatrix} \cos\theta & -\sin\theta \\ \sin\theta & \cos\theta \end{pmatrix} \qquad (2.15)$$

Here,

$$\theta = 45°$$

After rotation, the x and y axis become x$'$ and y$'$ respectively. Therefore,

$$\delta x' = \frac{\delta x}{\sqrt{2}} - \frac{\delta y}{\sqrt{2}}; \qquad (2.16)$$

$$\delta y' = \frac{\delta x}{\sqrt{2}} + \frac{\delta y}{\sqrt{2}}; \qquad (2.17)$$

The elements of the Hessian matrix were modified accordingly. The mass-weighted Hessian matrix $\mathbf{A}$ will have 3 eigenvectors $e_1, e_2,$ and e_3 and corresponding 3 eigenvalues will be λ_1, λ_2, and λ_3. For these eigenvalues, corresponding normal mode frequencies will be calculated using equation (2.4).

2.7   Zero-Point Energy

In classical mechanics, we assume that a collection of atoms always tends to relax to a state where the total energy of the material is minimum at 0 K. The coordinates of the atoms at this minimum energy or equilibrium state is called equilibrium positions. If the temperature is raised from 0 K, the atoms start vibrating about their equilibrium positions. But from quantum mechanical perspective, a collection of atoms not only has this minimum energy but also vibration around their equilibrium positions which contributes to the total energy of the material even at 0 K. This additional energy contribution due to vibration is known as Zero-Point Energy.

The concept of vibrational modes defined in previous section has been developed using harmonic approximation. In harmonic approximation, each vibrational mode can be represented by a harmonic oscillator. We can represent the potential energy of this oscillator as follows:

$$E = E_0 + \frac{k}{2}x^2. \tag{2.18}$$

In classical mechanics, the lowest energy of this oscillator is at x = 0 which is the equilibrium state. At this equilibrium state, kinetic energy becomes zero and the potential energy becomes E_0. But according to quantum mechanics, the lowest quantum mechanical energy will be:

$$E = E_0 + \frac{h\nu}{2} \tag{2.19}$$

Here, h is the plank's constant and ν is the classical vibrational frequency. The difference between this quantum mechanical energy and minimum energy according to classical mechanics gives the zero-point energy. Now if we apply this concept to a set of atoms, there will be zero-point energy contribution for each of the individual normal modes. The minimum energy considering all the normal modes is defined as:

$$E = E_0 + \sum_i \frac{h\nu_i}{2} \tag{2.20}$$

We will calculate E_0, the ground state total energy for the set of atoms using DFT code. Method to calculate ν_i, the normal mode frequencies using DFT was described in previous section.

2.8 Quantum Tunneling

According to transition-state theory, transition between two local energy minima happens only if the system gains enough energy to overcome the energy barrier at transition state. But quantum mechanics suggests that for particles with very small mass, transition may occur by the particle spontaneously passing through this barrier even though this particle energy is significantly lower than the energy barrier. This phenomenon is known as quantum tunneling. Due to very small mass, hydrogen atoms can quantum tunnel on various surfaces [37]. Quantum tunneling has been demonstrated with hydrogen on ice by making a comparison between diffusion rate of hydrogen and deuterium [38]. Quantum tunneling usually takes place at low temperature.

3. RESULTS AND DISCUSSION

3.1 Pd-Si Bond Length

Literature survey suggested Pd-Si bond length for PdSi, Pd_2Si and Pd_3Si phases investigated in different symmetry space groups [39]. In our DFT study, we adopted silicon crystal structure with symmetry space group: 'F d 3 m'. Therefore, we couldn't directly use the Pd-Si bond length reported in literature. The goal of our first DFT computation was to figure out Pd-Si bond length for 'F d 3 m' symmetry space group. This has a diamond structure with lattice constant, a = 5.43 Å, b = 5.43 Å, c = 5.43 Å. The symmetry space groups investigated in literature had different lattice parameters. Two of the space groups investigated in the literature for PdSi phase had cubic crystal structure. Diamond crystal structure is also cubic in nature but has additional atoms due to its inter-penetrating face centered cubic nature. We therefore evaluated the Pd-Si bond length using our DFT code ABINIT for these two cubic crystal structures. The lattice parameters were replaced by a value of 5.43 Å. This gave us the upper and lower bounds of Pd-Si bond length which had numeric values of 2.09 and 2.56 Å respectively.

Pd atom was placed in our Silicon supercell at the pore edge and allowed to form bond with nearby silicon atom. In the next step, we tried to relax this Pd-Si bond and determine actual Pd-Si bond length. In this relaxation approach, only the Pd atom was allowed to relax while all the silicon atoms were kept fixed. But since the number of atoms were pretty high (ie: 341 atoms), the computation didnt converge in reasonable amount of wall time in Big Red II. This led us to the second approach. We tried evenly spaced 8 different bond lengths between the lower and upper bounds. The bond length was varied between 2.09 and 2.56 Å as mentioned. Ground state total energy was computed for the 8 different bond lengths reported in table 3.1.

Table 3.1.

Ground State Total Energy comparison for different Pd-Si bond lengths

Pd-Si Bond Length (Å)	Total Energy (eV)
2.09	-6404.60
2.16	**-6404.70**
2.22	**-6404.70**
2.29	-6404.63
2.36	-6404.52
2.43	-6404.38
2.49	-6404.23
2.56	-6404.07

In above table, total GS (ground state) energy has been rounded up to two decimal places. Even though it shows equal energy for bond length of 2.16 and 2.22 Å, there is actually a small energy difference of 0.000455 eV. Therefore, we have used 2.16 Å as Si-Pd bond length for all subsequent work.

3.2 Catalyst Minimum Energy Location

3.2.1 Single Catalyst Atom

Summary of ground state energy DFT calculation for all 9 locations investigated as possible strategic location of single Pd catalyst atom in a quarter nanoporous silicon matrix is reported in table 3.2. Ground state total energy of location no. 9 is significantly lower compared to other 8 positions. This location was visualized in figure 2.9. Therefore, location 9 turns out to be the strategic location for catalyst placement. A careful review of this location reveals that this is a structurally weak location since the Pd catalyst is bonded to a silicon atom having only 2 neighboring silicon atoms. Consequently, this complies with the hypothesis regarding strategic

placement of the catalyst atom. This result also provides valuable insight in choosing possible location for Pd tetrahedron cluster deposition. It must be noted here that, we have used a Si-Pd bond length of 2.16 Å (Angstrom) calculated in previous section throughout our DFT computation.

Table 3.2.
Ground State Total Energy comparison for different locations of single
Pd Catalyst in a npSi matrix

Catalyst Location	Etotal (eV)
1	-41771.70
2	-41771.70
3	-41774.34
4	-41774.00
5	-41774.00
6	-41774.19
7	-41772.14
8	-41772.14
9	**-41775.30**

3.2.2 Multiple Catalyst Atom

The catalyst cluster is supposed to be supported on our nanoporous silicon matrix. Two different Pd-Pd bond lengths of 2.60 and 2.69 Å (Angstrom) have been reported in Pd tetrahedron structure supported in a substrate [26]. Therefore, we did compute ground state total energy for Pd cluster located at the three different proposed locations for bond length of 2.60 and 2.69 Å respectively. The summary of our DFT computations are presented here.

Table 3.3.

Ground State Total Energy Comparison for different locations of a Pd cluster in a npSi matrix

Catalyst Location	Pd-Pd bond length (Å)	Etotal (eV)
1	2.60	-32638.04
1	2.69	**-32638.19**
2	2.60	-32635.84
2	2.69	Unstable
3	2.60	-32637.20
3	2.69	-32637.10

It is evident that Pd tetrahedron with a Pd-Pd bond length of 2.69 Å located adjacent to the intersection of (100) and (110) plane is most stable in nature. We did further gaseous H_2 dissociation and spillover studies by keeping this as the strategic location for Pd catalyst cluster.

3.3 Dissociation Energy Barrier

Literature survey suggests that single Pd catalyst atom supported on hydrogen storage material adsorbs 2 molecular H_2 [40]. Even though previous work suggests 4 different structures, the most favorable coordination structure of this H_2 adsorbed Pd is very similar to PdH_2 complex where the H-H bond is not completely dissociated, rather extended [41]. This Pd-dihydrogen complex is called Kubas complex [42]. In this coordination structure, the observed H-H bond length is in the range of 0.85-0.87 Å, Pd-H bond length is 1.75 Å, and the H-Pd-H angle lies between 28 to 29° [41]. In our hydrogen dissociative adsorption study, we have maintained a H-H bond length of 0.85 Å. Pd-H bond length and H-Pd-H angle is set to 1.75 Å and 28.2°. The ground state total energy of this configuration was computed using ABINIT. The difference between the ground state total energy of the system when H_2 is 15 Å away and

the total energy when the porous silicon matrix contains PdH_2 structure gives the dissociation energy barrier. The computed ground state total energy values for these two cases were -41830.52 and -41832.44 eV. Therefore, the dissociative adsorption barrier is 1.92 eV which is quite large relative to thermal energy in temperature ranges of interest. This high energy barrier raised the necessity of investigating hydrogen dissociation on multiple catalyst atoms forming a cluster.
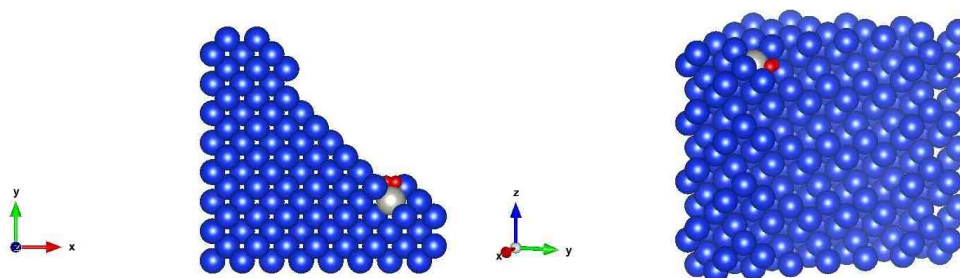
Fig. 3.1. Dissociative Adsorption of H_2 on a Single Pd Atom: top view (left) and side view (right).

Previous DFT work suggested that catalyst clusters consisting of small number of atoms have the ability to reduce the energy barrier for H_2 dissociation on this metal cluster [43] [44]. Such studies were limited to catalyst structures consisting of maximum 3 atoms. Since in our case we have catalyst cluster consisting of 4 atoms, we decided to investigate the impact of Pd cluster consisting of 4 atoms on the H_2 dissociation energy barrier. Moc et al. have demonstrated that H_2 is dissociated on a Pd_4 cluster and the dissociated hydrogen atoms that bridge the Pd-Pd edges not sharing the Pd atom in a Pd tetrahedron is most favorable [45]. The Pd-Pd bond length was kept same as the Pd-Pd bond length in a ground state Pd_4 structure which is 2.69 Å. We configured Pd_4H_2 structures accordingly where the dissociated H atoms are placed at equal distance of 1.66 Å from the Pd atoms forming a Pd-Pd edge. In total, there are two such Pd-Pd edges and these edges don't share any Pd atom. For

our nanoporous silicon matrix, three such configurations were made. In two of them, the dissociated hydrogen atom gets within Si-H bond length and therefore discarded. As a result, we could study only one configuration. It's demonstrated in figure 3.2.
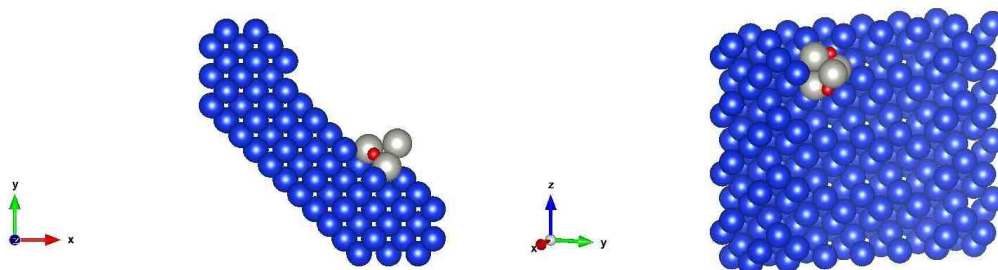
Fig. 3.2. H_2 dissociation on Pd tetrahedron cluster: top view (left) and side view (right).

The ground state total energy was computed for before and after hydrogen dissociation phase just like single catalyst atom study. The before and after dissociation ground state total energy values were -32669.14 and -32669.61 eV. This gave a reduced hydrogen dissociation energy barrier of 0.47 eV which is significantly lower than the energy barrier value computed in single catalyst atom study. It was then recommended to the experimental researchers to use clusters of catalyst atoms instead of single atoms.

3.4   Spillover Energy Barrier

In single catalyst atom case, we investigated hydrogen spillover from the Pd atom to the silicon dangling bonds located at adjacent silicon surface. These silicon atoms should have a coordination number lower than 4. To find out suitable silicon dangling bonds for the spilled over hydrogen atoms, we carefully looked into all the nearby silicon atoms that match this criteria. There were 3 silicon atoms with lower coordination number than 4 in a very close proximity to these relaxed hydrogen atoms.

They had coordination numbers of 1, 2, and 3 respectively. Among these 3 atoms, the lower two coordination number silicon atoms were closest to the Pd atom. Therefore, we chose these two silicon atoms for spillover. The Si-H bond length was kept 1.48 Å [46] for all studies involving Si-H bond. The total ground state energy was computed using ABINIT. Hydrogen atoms have to overcome an energy barrier for spillover. The energy difference between the state before spillover and after spillover provides the spillover energy barrier. From the DFT computation, the ground state total energy of the system before and after spillover had a values of -41830.52 and -41832.36 eV respectively. Therefore, there exists an energy barrier of 1.84 eV for spillover.

This spillover energy barrier for single catalyst atom turned out quite large relative to thermal energy in temperature ranges of interest. So, we decided to initiate spillover investigation for multiple catalyst cluster. As mentioned in catalyst study section, catalyst structures are supposed to raise H potential to spillover favorable range [26]. Since the Pd atoms forming the tetrahedron lands on some of the lower coordination silicon atoms at the surface, we didn't have any silicon atoms with coordination number 1 available for spillover in our system. But, there were silicon atoms with coordination number 2 and 3 available for spillover. We included all 3 of these nearby silicon atoms in this spillover study. Two of them had coordination number 2 whereas the other atom had a coordination number of 3. Figure 3.3 and 3.4 demonstrate the state of the matrix after hydrogen spillover from catalyst cluster. Corresponding ground state total energy computed using ABINIT is listed in table 3.4.

Table 3.4.
Spillover Barrier for Hydrogen Spillover from Pd cluster located at npSi matrix

Serial	Energy Before Spillover (eV)	Energy After Spillover (eV)	Spillover Barrier (eV)
1	-32669.61	-32670.21	0.60
2		-32670.10	0.49
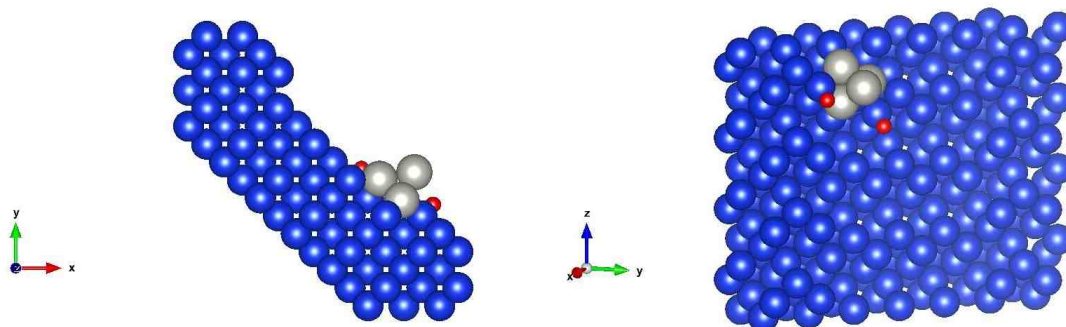
Fig. 3.3. After Spillover from Pd Cluster: split hydrogen forms bond with low valence silicon located at nearby surface; top view (left) and side view (right).
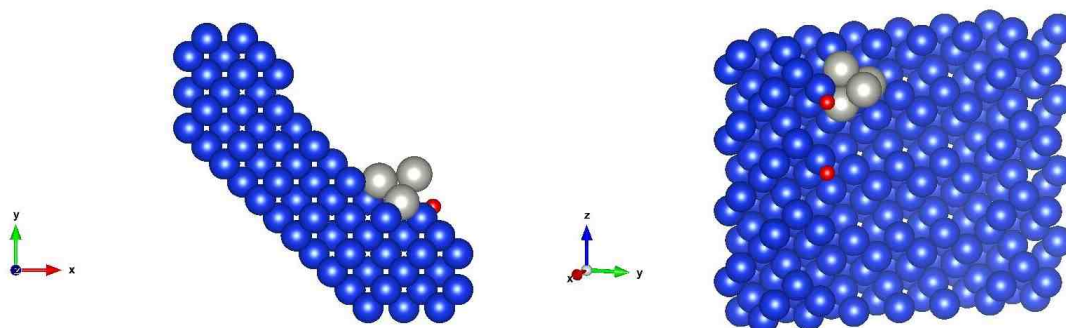
Fig. 3.4. After Spillover from Pd Cluster: split hydrogen forms bond with low valence silicon located at nearby surface; top view (left) and side view (right).

The energy barrier for spillover from Pd cluster is considerably lower than energy barrier from single Pd catalyst atom. Note that, even though hydrogen atom has to overcome a lower spillover barrier in second configuration listed in table 3.4, the dangling silicon atom is located almost 1 unit cell away from the Pd cluster. Therefore, it is more likely that spillover will occur as per configuration 1 with a spillover barrier of 0.60 eV.

3.5 Energy Difference between Recharged and Discharged State

In following table, we have summarized the DFT results of hydrogen recharged-discharged state described in section 2.4. The completely recharged state refers to 102 numbers of hydrogen atoms in solid state and no gaseous H_2 molecule in the vacuum. On the other hand, the completely discharged state refers to 51 numbers of H_2 in vacuum and no hydrogen atom in solid state. Apart from these completely recharged and completely discharged states, we also studied 3 intermediate states. In these intermediate states, hydrogen is present in the system as both gas and solid. The total number of hydrogen atoms in the system including both gas and solid are fixed throughout this study. In each of this intermediate states, 24 to 26 hydrogen atoms are removed from vacuum and turned to solid state. This represents 25% incremental recharge. Consequently, the intermediate states are in fact 25%, 50%, and 75% recharged state. We used a random number generator function to choose atoms to recharge into this storage medium. This process was repeated 6 times resulting in the 6 samples in the left most column of table 3.5. The ground state total energy was computed using ABINIT in all the cases.

Table 3.5.: Ground State Energy Comparison for Different Recharge Scenarios

Sample	Recharge(%)	Number of H_2 Molecules	Number of Solid H Atom	Total Energy (Ha)
	0	51	0	-1594.18
	25	38	26	-1593.76
1	50	26	50	-1592.70
	75	13	76	-1591.97
	100	0	102	-1592.79
	0	51	0	-1594.18
	25	38	26	-1594.48
2	50	26	50	-1594.09

Table 3.5.: *continued*

Sample	Recharge(%)	Number of H_2 Molecules	Number of Solid H Atom	Total Energy (Ha)
	75	13	76	-1592.37
	100	0	102	-1592.79
3	0	51	0	-1594.18
	25	38	26	-1594.50
	50	26	50	-1594.09
	75	13	76	-1593.11
	100	0	102	-1592.79
4	0	51	0	-1594.18
	25	38	26	-1594.48
	50	26	50	-1593.38
	75	13	76	-1592.64
	100	0	102	-1592.79
5	0	51	0	-1594.18
	25	38	26	-1594.12
	50	26	50	-1594.04
	75	13	76	-1593.37
	100	0	102	-1592.79
6	0	51	0	-1594.18
	25	38	26	-1593.38
	50	26	50	-1593.00
	75	13	76	-1593.01
	100	0	102	-1592.79

The ground state total energy for different hydrogen recharge scenarios computed in ABINIT was plotted against recharge percentage in MATLAB for all 6 samples. Next, we took average values of the ground state energy of each loading scenario over all the samples and plotted against recharge percentage. The following plot includes original and average energy values. The thick line represents the average values.
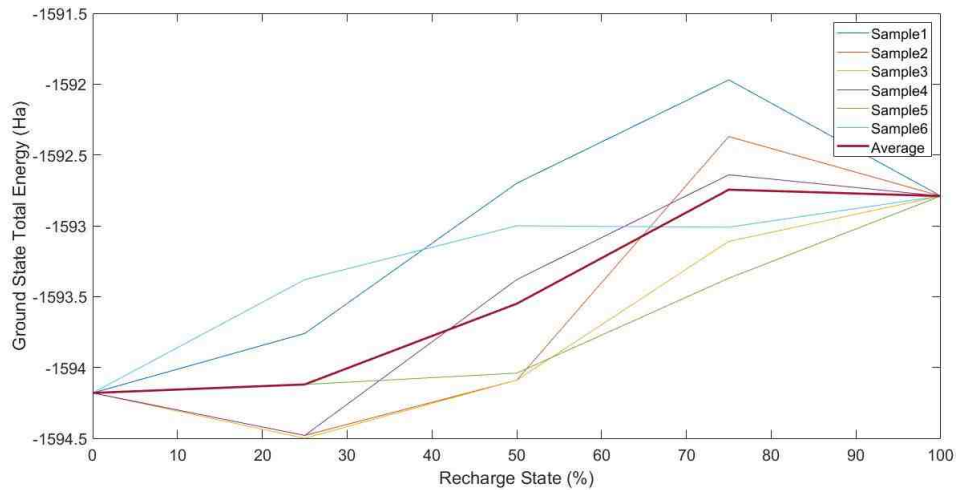
Fig. 3.5. Ground State Total Energy (Ha) vs Recharge State (%)

From the tabulated data and the MATLAB plot, we see an energy difference of 0.01 Ha/atom which is equivalent to 0.38 eV/atom between fully recharged and fully discharged porous silicon matrix. This is the amount of energy we need to provide from external sources for example pressure and temperature to recharge the storage medium from complete hydrogen empty state. As described in section 2.4, the H_2 molecules were forced close together for easier plane wave solution. But this arrangement might have led to interaction between the H_2 molecules. This implies high pressure in the storage system and is one of the probable reasons behind such high energy requirement to charge the storage medium from hydrogen depleted state.

3.6 Bond Hopping Energy Barrier

3.6.1 Single Hop

Below we listed the energy different between the images evaluated in NEB method for direct single hop. From the data it's evident that hydrogen atom will have to overcome an energy barrier of 2.06 eV to make a direct hop of distance 5.43 Å. This is quite big barrier for hydrogen atom to overcome. Therefore, it will probably opt for the alternate bond hopping path consisting of two sequential hops instead of one direct hop.

Table 3.6.
Ground State Total Energy Difference between Images for Direct Hop
from Initial to Final State.

Image	Energy Difference (eV)
1	0.10
2	0.52
3	1.43
4	2.01
5	**2.06**
6	1.94
7	1.87
8	1.83
9	1.79
10	1.09
11	0.53
12	0.14
13	0.00

3.6.2   Double Hop

In table 3.7 and 3.8, we listed the energy difference between the images evaluated in Improved Tangent NEB method for double hop. First table refers to the data of the first hop and the data listed in second table is of the second hop. For the first hop, the transition state gives an energy barrier of 1.74 eV. The energy barrier value is 1.45 eV for the second hop. These values are smaller compared to the energy barrier of direct bond hop case. Therefore, we can conclude that hydrogen atom will preferentially diffuse along the silicon surface by bond hopping process consisting of two sequential diagonal hops along the crystal face in order to cover a vertical bond hopping distance of 5.43 Å. Energy barrier vs Bond hopping distance is plotted in MATLAB in figure 3.6 for both direct and indirect bond hopping pathways.

Table 3.7.
Ground State Total Energy Difference (eV) between Images for First
Hop from Initial to Quasi Stable State.

Image	Energy Difference (eV)
1	0.03
2	0.31
3	0.96
4	1.52
5	**1.74**
6	1.47
7	0.87
8	0.25
9	0.00

Table 3.8.

Ground State Total Energy Difference (eV) between Images for Second Hop from Quasi Stable State to Final State

Image	Energy Difference (eV)
1	0.06
2	0.62
3	**1.45**
4	0.54
5	0.00

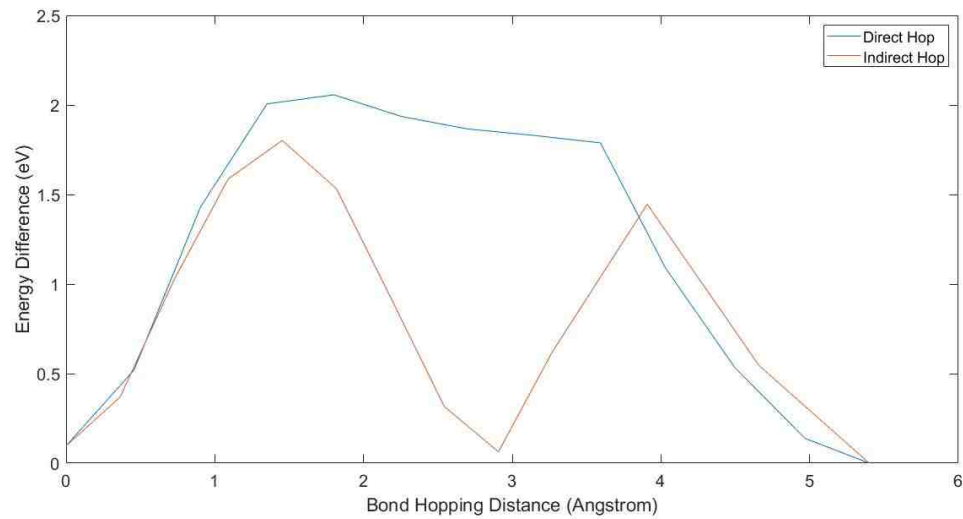Fig. 3.6. Energy Barrier (eV) vs Bond Hopping Distance (Å)

3.7   Diffusion

In order to figure out the vibrational modes and corresponding vibrational frequencies, we initially calculated the ground state total energy at local minimum using ABINIT. This is the E(x,y,z) value as defined in Method section. To determine the value of the energy components specified in equation (2.6) through (2.11), we need to

do ground state total energy computation for each of the individual components of right hand side of the equations where the H atom is moved along x or y or z and/or their combinations by δx, δy, δz etc. These values were chosen as 0.04 Å as suggested in literature for good convergence [10]. Once we compute these energy values, we can generate the Hessian matrix. Since we are mainly interested in mass weighted Hessian matrix, each of the components of Hessian matrix was divided by the mass of hydrogen atom, m = 1.67×10^{-27} Kg. This gives us the mass weighted Hessian matrix, $\mathbf{A}$.

At local minimum, these matrix had following components:

$$\mathbf{A} = \begin{pmatrix} 1.04 \times 10^{28} & -7.90 \times 10^{25} & 5.66 \times 10^{25} \\ -7.90 \times 10^{25} & 9.2 \times 10^{28} & -6.61 \times 10^{28} \\ 5.66 \times 10^{25} & -6.61 \times 10^{28} & 6.37 \times 10^{28} \end{pmatrix}$$

From this matrix we retrieved the eigenvalues using MATLAB *eig* function. Corresponding eigenvalues are: $\lambda_1 = 0.1026 \times 10^{29}$, $\lambda_2 = 0.1040 \times 10^{29}$, and $\lambda_3 = 1.4547 \times 10^{29}$. When we put this eigenvalues in equation (2.4), it gave us following vibrational frequency values at local minimum:

$\nu_1 = 1.61 \times 10^{13}$ s^{-1}, $\nu_2 = 1.62 \times 10^{13}$ s^{-1}, and $\nu_3 = 6.07 \times 10^{13}$ s^{-1}.

We can see that the ν_3 value is highest among the three normal modes. These results denote fastest diffusion along vertical direction but diffusion in lateral direction is also sizable. Over time, our npSi charged with impure hydrogen will include poisons which occupy dangling bond sites making them unavailable for bond hopping. Since the lateral movement is not much slower than vertical, hydrogen will still be able to move around poisoned sites. This may slightly slow down the recharge/discharge, and slightly reduce the capacity, but provides robustness to this method of hydrogen storage.

3.8 Zero-Point Energy Corrections

In previous section, we have figured out bond hopping energy barrier using Nudged Elastic Band (NEB) Method. NEB evaluates energy barrier from classical mechanics perspective. It doesn't include zero-point energy corrections. This zero-point energy correction is particularly important for system having light atoms [10]. Since our system involves hydrogen atoms, inclusion of zero-point energy correction may have significant impact on the bond hopping energy barrier. In order to find zero-point energy corrected activation energy, we will need to include zero-point energy corrections for both energy minima and transition state. In any set of atoms having N degrees of freedom, there will be N-1 real vibrational modes and 1 (one) imaginary mode at transition state whereas the local minimum will have N real vibrational modes [10]. The following equation gives zero-point energy corrected activation energy accordingly:

$$\Delta E_{ZP} = \left(E^\dagger + \sum_{j=1}^{N-1} \frac{h\nu_j^\dagger}{2} \right) - \left(E_A + \sum_{i=1}^{N} \frac{h\nu_i}{2} \right) \tag{3.1}$$

Here, $E^\dagger$ and E_A represents ground state total energy at transition state and energy minima respectively. Their difference denotes the activation energy, ΔE defined in classical mechanics. In the above equation, ν_i and ν_j defines the normal mode frequencies at local minimum and transition states respectively. The above equation can be re-written as:

$$\Delta E_{ZP} = \Delta E + \sum_{j=1}^{N-1} \frac{h\nu_j^\dagger}{2} - \sum_{i=1}^{N} \frac{h\nu_i}{2} \tag{3.2}$$

Since in our system, the hydrogen atom has 3 degrees of freedom, the transition state will have 2 real vibrational modes and 1 imaginary mode. The local minimum will have all 3 real vibrational modes. In our alternate double hop NEB study, the energy barrier value was 1.74 eV for the first hop. Using the method defined in previous section, we calculated all these vibrational modes using ABINIT at both local minimum and the transition state.

Normal mode frequency values at local minimum were already computed in previous section. We are calculating those values at transition state. The mass weighted Hessian matrix consists of following components:

$$\mathbf{A} = \begin{pmatrix} 2.72 \times 10^{27} & 6.10 \times 10^{27} & -1.50 \times 10^{28} \\ 6.10 \times 10^{27} & 3.57 \times 10^{27} & 1.48 \times 10^{28} \\ -1.50 \times 10^{28} & 1.48 \times 10^{28} & -2.857 \times 10^{28} \end{pmatrix}$$

Corresponding eigenvalues were as follows: $\lambda_1^{\dagger}$ = -4.0345×10^{28}, $\lambda_2^{\dagger}$ =0.8762×10^{28} , and $\lambda_3^{\dagger}$ = 0.9423×10^{28}. Using the same equation (2.4) we get the frequency values: $\nu_1^{\dagger} = 1.49 \times 10^{13}$ s^{-1}, $\nu_2^{\dagger} = 1.54 \times 10^{13}$ s^{-1}. Even though we don't need the imaginary mode frequency for zero-point energy, the value turned out as, $\nu_{Im}^{\dagger} = 3.20 \times 10^{13}$ s^{-1}. Plank constant, h = 4.14×10^{-15} eV.s. Putting all these values in equation (3.2) we get,

$$\Delta E_{ZP} = 1.58 eV.$$

This gives the zero-point corrected bond hopping energy barrier for the first hop. This value is 0.16 eV lower than the bond hopping barrier calculated using classical mechanics. The zero-point corrected activation energy can be calculated for the second hop using the same approach.

Diffusion coefficient can be calculated using these values in following equation:

$$D = \frac{1}{z}\nu_e \alpha^2 exp(-\frac{E_a}{kT}) \tag{3.3}$$

Here, ν_e is the effective vibrational frequency. The direction of first bond hop closely aligns with z-coordinate whereas for second hop it's aligned with x-coordinate. Therefore, we choose ν_e values of 6.07×10^{13} s^{-1} and 1.61×10^{13} s^{-1} respectively. z represents the coordination number which is 4. The hopping distance and activation energy are represented by α and E_a respectively. For first hop, α = 4.50 Å. α value is 2.35 Å for second hop. At 100°C the kinetic energy value is 0.048 eV. Plugging all these values in equation (3.3) we get diffusion coeefficient values for first and second

hop: $D_{1^{st}hop} = 1.56 \times 10^{-20} m^2/s$, $D_{2^{nd}hop} = 1.69 \times 10^{-20} m^2/s$. Note that, activation energy values of 1.58 and 1.45 eV were considered for first and second hop. The surface diffusion is likely be limited by $1.56 \times 10^{-20} m^2/s$.

3.9 Quantum Tunneling

Hydrogen diffusion for hydrogen storage applications may happen by bond hopping and quantum tunneling [47]. The impact of quantum tunneling on overall diffusion rate is controlled by crossover temperature. Below this crossover temperature, hydrogen passes through local minimas by quantum tunneling procedure. Above this temperature, hydrogen atom has to overcome the huge energy barrier for diffusion along the silicon surface. Crossover temperature is defined in following equation:

$$T_c = \frac{h\nu_{Im}^{\dagger} E_{ZP}/k_B}{2\pi E_{ZP} - h\nu_{Im}^{\dagger} ln2} \tag{3.4}$$

Here, $\nu_{Im}^{\dagger}$ denotes the imaginary frequency at transition state. E_{ZP} and k_B represents the zero-point energy corrected activation energy and Boltzmann constant respectively. $k_B = 8.62 \times 10^{-5}$ eVK^{-1}. Putting the value of h, $\nu_{Im}^{\dagger}$, E_{ZP} defined in previous section into above equation we find this crossover temperature value for our hydrogen storage system.

$$T_c = 246.38K.$$

We anticipate that the operating temperature of our storage media will be close to room temperature. Since the crossover temperature is below room temperature, quantum tunneling won't impact hydrogen diffusion in this storage media.

4. SUMMARY

4.1 Conclusion

In this thesis, density functional theory (DFT) study was carried out to investigate hydrogen coverage, dissociation, spillover, bond hopping, and diffusion phenomena in nanoporous silicon matrix. The computed dissociation, spillover, and bond hopping energy barrier values were 0.47, 0.60, 1.74 eV (first hop), and 1.45 eV (second hop) respectively. The bond hopping energy barrier further reduced to 1.58 eV (first hop) when we incorporated zero-point energy corrections. Tetrahedron Pd catalyst cluster lowered the hydrogen dissociation and spillover energy barrier by 1.45 and 1.24 eV respectively compared to single Pd atom. It has been demonstrated that the spilled over hydrogen atoms will jump preferentially from current silicon dangling bond to next available silicon dangling bonds in two sequential hops: first hop diagonally along crystal face at a distance of 4.50 Å and the second hop at a distance of 2.35 Å. The value of computed energy barrier for the first hop is 1.58 eV after zero-point energy correction. The hydrogen diffusion along pore depth shows a much higher vibrational frequency of 6.07×10^{13} s^{-1}. Since our pore is much longer in the z-direction than x- and y-directions, fast diffusion along pore depth is a positive attribute for the storage media. The evaluated crossover temperature suggests that quantum tunneling won't play any significant role since the crossover temperature is below room temperature and much lower than the anticipated operating temperature of our storage media. Thus, bond hopping will dominate in the hydrogen diffusion rate in nanoporous silicon. This dissociation energy barrier is within the range of 0.20 eV to 0.60 eV preferred for any hydrogen storage media [48]. The calculated

vibrational frequency is higher than the reported frequency of 10^{12} to $10^{13}s^{-1}$ [49]. These microscopic results predicts the feasibility of nanoporous silicon as a viable hydrogen storage medium.

4.2   Future Work

We suggest following studies to be carried out in future to improve upon the work depicted within the scope of this thesis:

1. Bond hopping activation energy study using Nudged Elastic Band (NEB) method can be performed with more intermediate points and lower tolerance to find out more accurate or exact location of the transition state. This will provide actual or near precise activation energy.

2. Different phenomenon regarding only hydrogen recharge has been included within the scope of this thesis, hydrogen discharge as a means of both desorption and reverse spillover mechanism may be studied to evaluate the feasibility for complete recharge-discharge cycle.

3. We have considered only a quarter of hexagonal pore in our DFT study where the pore is consistent in shape. The actual shape of pore in as synthesized porous silicon may have different irregularities. The irregularities may be incorporated in our DFT study to have the actual pore morphology.

4. It is possible that other Pd atoms motile (movable) on the silicon surface may migrate towards these Pd clusters and cause them to agglomerate and become bigger. A future study should look into this.

5. To obtain precise energy value required to recharge the storage media from complete hydrogen depleted state, future research should investigate a larger supercell for charge-discharge. That way high pressure condition can be avoided by allowing the H_2 molecules to be away from each other. Alternate could be to place more H_2 molecules over silicon. But this may require more powerful supercomputer facility.

6. In this study ABINIT default LDA based exchange-correlation functional was used. LDA based other popular exchange-correlation functionals may be used and a comparison study can be done between the results retrieved for different exchange-correlation functionals.

7. All the calculations are done in 0K in DFT. At 0K, bond reformation doesn't take place. Future study should incorporate the effect of non-zero temperature.

REFERENCES

REFERENCES

[1] L. Schlapbach and A. Züttel, "Hydrogen-storage materials for mobile applications," in *Materials For Sustainable Energy: A Collection of Peer-Reviewed Research and Review Articles from Nature Publishing Group*. World Scientific, 2011, pp. 265–270.

[2] G. W. Crabtree, M. S. Dresselhaus, and M. V. Buchanan, "The hydrogen economy," *Physics Today*, vol. 57, no. 12, pp. 39–44, 2004.

[3] P. Schubert and A. Wilks, "Thermodynamic analysis of a novel hydrogen storage material: Nanoporous silicon," *Materials Innovations in an Emerging Hydrogen Economy*, vol. 202, p. 105, 2009.

[4] J. Li, T. Furuta, H. Goto, T. Ohashi, Y. Fujiwara, and S. Yip, "Theoretical evaluation of hydrogen storage capacity in pure carbon nanostructures," *The Journal of chemical physics*, vol. 119, no. 4, pp. 2376–2385, 2003.

[5] "Nsf award search: Award # 1648748 - sttr phase i: Hydrogen storage in catalytically-modified porous silicon," https://www.nsf.gov/awardsearch/showAward?AWD_ID=1648748, accessed: 2017-01-15.

[6] "American mineralogist crystal structure database," http://rruff.geo.arizona.edu/AMS/minerals/Silicon.htm, accessed: 2017-02-10.

[7] "Gordon group/gamess homepage," http://www.msg.ameslab.gov/gamess/, accessed: 2016-08-03.

[8] "Abinit," https://www.abinit.org, accessed: 2016-12-18.

[9] S. Goedecker, M. Teter, and J. Hutter, "Separable dual-space gaussian pseudopotentials," *Physical Review B*, vol. 54, no. 3, p. 1703, 1996.

[10] D. Sholl and J. A. Steckel, *Density functional theory: a practical introduction*. John Wiley & Sons, 2011.

[11] S. Banerjee, C. Pillai, and C. Majumder, "Dissociation and diffusion of hydrogen on the mg (0001) surface: catalytic effect of v and ni double substitution," *The Journal of Physical Chemistry C*, vol. 113, no. 24, pp. 10 574–10 579, 2009.

[12] H. J. Monkhorst and J. D. Pack, "Special points for brillouin-zone integrations," *Physical review B*, vol. 13, no. 12, p. 5188, 1976.

[13] N. Troullier and J. L. Martins, "Efficient pseudopotentials for plane-wave calculations," *Physical review B*, vol. 43, no. 3, p. 1993, 1991.

[14] "Pseudopotentials - quantumespresso," http://www.quantum-espresso.org/pseudopotentials/, accessed: 2017-02-09.

[15] "Big red ii at indiana university," https://kb.iu.edu/d/bcqt.htm, accessed: 2016-09-06.

[16] F. Bottin, S. Leroux, A. Knyazev, and G. Zérah, "Large-scale ab initio calculations based on three levels of parallelization," *Computational Materials Science*, vol. 42, no. 2, pp. 329–336, 2008.

[17] "Parallelism for the ground state," https://www.abinit.org/sites/default/files/last/tutorial/generated_files/lesson_paral_gspw.html, accessed: 2017-02-10.

[18] J. Rodriguez, "Physical and chemical properties of bimetallic surfaces," *Surface Science Reports*, vol. 24, no. 7-8, pp. 223–287, 1996.

[19] J. G. Speight *et al.*, *Lange's handbook of chemistry.* McGraw-Hill New York, 2005, vol. 1.

[20] M. Arai, M. Fukushima, and Y. Nishiyama, "Interrupted-temperature programmed desorption of hydrogen over silica-supported platinum catalysts: the distribution of activation energy of desorption and the phenomena of spillover and reverse spillover of hydrogen," *Applied surface science*, vol. 99, no. 2, pp. 145–150, 1996.

[21] O. Alexeev, D.-W. Kim, G. W. Graham, M. Shelef, and B. C. Gates, "Temperature-programmed desorption of hydrogen from platinum particles on γ-al2o3: Evidence of platinum-catalyzed dehydroxylation of γ-al2o3," *Journal of catalysis*, vol. 185, no. 1, pp. 170–181, 1999.

[22] V. Lysenko, F. Bidault, S. Alekseev, V. Zaitsev, D. Barbier, C. Turpin, F. Geobaldo, P. Rivolo, and E. Garrone, "Study of porous silicon nanostructures as hydrogen reservoirs," *The journal of physical chemistry B*, vol. 109, no. 42, pp. 19 711–19 718, 2005.

[23] P. J. Schubert, "Solid-state hydrogen storage media and catalytic hydrogen recharging thereof," August 27 2013, US Patent 8,518,856.

[24] P. Schubert and A. Urbanek, "Hydrogen recharge dynamics and vessel design for porous silicon storage media," *Proceedings of TechConnect World 2014*, 2014.

[25] W. C. Conner Jr and J. L. Falconer, "Spillover in heterogeneous catalysis," *Chemical reviews*, vol. 95, no. 3, pp. 759–788, 1995.

[26] A. K. Singh, M. A. Ribas, and B. I. Yakobson, "H-spillover through the catalyst saturation: an ab initio thermodynamics study," *Acs Nano*, vol. 3, no. 7, pp. 1657–1662, 2009.

[27] C. Zhou, J. Wu, A. Nie, R. C. Forrey, A. Tachibana, and H. Cheng, "On the sequential hydrogen dissociative chemisorption on small platinum clusters: a density functional theory study," *The Journal of Physical Chemistry C*, vol. 111, no. 34, pp. 12 773–12 778, 2007.

[28] L. Chen, A. C. Cooper, G. P. Pez, and H. Cheng, "Density functional study of sequential h2 dissociative chemisorption on a pt6 cluster," *The Journal of Physical Chemistry C*, vol. 111, no. 14, pp. 5514–5519, 2007.

[29] A. D. Lueking and R. T. Yang, "Hydrogen spillover to enhance hydrogen storagestudy of the effect of carbon physicochemical properties," *Applied Catalysis A: General*, vol. 265, no. 2, pp. 259–268, 2004.

[30] E. Weinan, W. Ren, and E. Vanden-Eijnden, "String method for the study of rare events," *Physical Review B*, vol. 66, no. 5, p. 052301, 2002.

[31] E. Weinan, W. Ren, and E. Vanden-Eijnden, "Simplified and improved string method for computing the minimum energy paths in barrier-crossing events," *Journal of Chemical Physics*, vol. 126, no. 16, p. 164103, 2007.

[32] "Tutorial paral string," https://www.abinit.org/sites/default/files/infos/7.6/tutorial/lesson_paral_string.html, accessed: 2017-11-19.

[33] H. Jónsson, G. Mills, and K. W. Jacobsen, "Nudged elastic band method for finding minimum energy paths of transitions," in *Classical and quantum dynamics in condensed phase simulations*. World Scientific, 1998, pp. 385–404.

[34] G. Henkelman, B. P. Uberuaga, and H. Jónsson, "A climbing image nudged elastic band method for finding saddle points and minimum energy paths," *The Journal of chemical physics*, vol. 113, no. 22, pp. 9901–9904, 2000.

[35] G. Henkelman and H. Jónsson, "Improved tangent estimate in the nudged elastic band method for finding minimum energy paths and saddle points," *The Journal of chemical physics*, vol. 113, no. 22, pp. 9978–9985, 2000.

[36] M. Dürr and U. Höfer, "Hydrogen diffusion on silicon surfaces," *Progress in Surface Science*, vol. 88, no. 1, pp. 61–101, 2013.

[37] J. T. Fermann and S. Auerbach, "Modeling proton mobility in acidic zeolite clusters: Ii. room temperature tunneling effects from semiclassical rate theory," *The Journal of Chemical Physics*, vol. 112, no. 15, pp. 6787–6794, 2000.

[38] K. Kuwahata, T. Hama, A. Kouchi, and N. Watanabe, "Signatures of quantum-tunneling diffusion of hydrogen atoms on water ice at 10 k," *Physical review letters*, vol. 115, no. 13, p. 133201, 2015.

[39] P. Turchi and V. Ivashchenko, "First-principles study of the pd–si system and pd (001)/sic (001) hetero-structure," *Journal of Nuclear Materials*, vol. 454, no. 1, pp. 308–314, 2014.

[40] S. Dag, Y. Ozturk, S. Ciraci, and T. Yildirim, "Adsorption and dissociation of hydrogen molecules on bare and functionalized carbon nanotubes," *Physical Review B*, vol. 72, no. 15, p. 155404, 2005.

[41] I. Lopez-Corral, E. German, A. Juan, M. A. Volpe, and G. P. Brizuela, "Dft study of hydrogen adsorption on palladium decorated graphene," *The Journal of Physical Chemistry C*, vol. 115, no. 10, pp. 4315–4323, 2011.

[42] G. J. Kubas, "Metal–dihydrogen and σ-bond coordination: the consummate extension of the dewar–chatt–duncanson model for metal–olefin π bonding," *Journal of Organometallic Chemistry*, vol. 635, no. 1-2, pp. 37–68, 2001.

[43] Q. Cui, D. G. Musaev, and K. Morokuma, "Molecular orbital study of h 2 and ch 4 activation on small metal clusters. i. pt, pd, pt 2, and pd 2," *The Journal of chemical physics*, vol. 108, no. 20, pp. 8418–8428, 1998.

[44] Q. Cui, D. G. Musaev, and K. Morokuma, "Molecular orbital study of h2 and ch4 activation on small metal clusters. 2. pd3 and pt3," *The Journal of Physical Chemistry A*, vol. 102, no. 31, pp. 6373–6384, 1998.

[45] J. Moc, D. G. Musaev, and K. Morokuma, "Adsorption of multiple h2 molecules on pd3 and pd4 clusters. a density functional study," *The Journal of Physical Chemistry A*, vol. 104, no. 49, pp. 11 606–11 614, 2000.

[46] "Common bond energies," http://www.wiredchemist.com/chemistry/data/bond_energies_lengths.html, accessed: 2017-01-31.

[47] B. Bhatia and D. S. Sholl, "Quantitative assessment of hydrogen diffusion by activated hopping and quantum tunneling in ordered intermetallics," *Physical Review B*, vol. 72, no. 22, p. 224302, 2005.

[48] H. Xiao, S. Li, and J. Cao, "First-principles study of pd-decorated carbon nanotube for hydrogen storage," *Chemical Physics Letters*, vol. 483, no. 1-3, pp. 111–114, 2009.

[49] J. Owen, D. Bowler, C. Goringe, K. Miki, and G. Briggs, "Hydrogen diffusion on si (001)," *Physical Review B*, vol. 54, no. 19, p. 14153, 1996.